Investigating the utility of a linear sea ice drift model for the Arctic

Javier Mozo

Master in Oceanography
60 credits

MetOs
Department or Geosciences

UNIVERSITY OF OSLO

January 2017

"And now there came both mist and snow,
And it grew wondrous cold:
And ice, mast-high, came floating by,
As green as emerald.
And through the drifts the snowy clifts
Did send a dismal sheen:
Nor shapes of men nor beasts we ken—
The ice was all between.
The ice was here, the ice was there,
The ice was all around:
It crack'd and growl'd, and roar'd and howl'd,'
Like noises in a swound!"

Samuel Taylor Coleridge, "The rhyme of the ancient mariner" (1798)

OSLO UNIVERSITY

Abstract

The Faculty of Mathematics and Natural Sciences
Department or Geosciences

Master in Oceanography

Investigating the utility of a linear sea ice drift model for the Arctic

by Javier MOZO

[Thorndike and Colony, 1982] have shown that the relationship between the drift of sea ice and the wind can be modelled by a linear equation when internal sea ice stresses are neglected. We investigate the usefulness of this linear model for sea ice drift in order to predict the time-evolving sea ice velocity from time-evolving surface winds and steady geostrophic ocean currents. We elaborate on the otherwise limited evaluation of the validity of the model. The results are assessed with respect to a priori assumptions, i.e. neglected sea ice stress (in relation to ice thickness or the effect of coasts) or sea currents variability. We have also analysed the possible correlation between the residuals and the wind. The main objective is to provide MET Norway with good enough estimates of the uncertainty associated with this model to supplement its own estimates and achieve better predictions.

Acknowledgements

I thank first and foremost my supervisor, Pål Erik Isachsen. Choosing you to guide me through this experience is one of the best decision I've taken in my life.

I want to thank also my co-supervisors. Thomas Lavergne and Jens Debernard, for their help.

And of course, this wouldn't have been possible without my family.

Contents

List of Figures

List of Tables

Chapter 1

The frozen ocean

"Land properly speaking no longer exists, nor sea nor air, but a mixture of these things, like a marine lung in which earth and water and all things are in suspension"

Pytheas of Massalia, "On the ocean"
(Believed to be the first Westerner to document sea ice around 325 BC)

1.1 "Solid state oceanography"[1]

Sea ice occurs in about 12% of the world ocean's surface [Weeks, 2010], most of it covering the Arctic and Antarctic oceans above 60^{o} of latitude. It is a conspicuous, year-round feature in the polar oceans that introduces a particular interface between the atmospheric and oceanic boundary layers and has a profound impact in the exchange of momentum, heat and material between the atmosphere and the ocean at high latitudes [Leppäranta, 2011].

The polar oceans are not covered by a continuously uniform sheet of ice. Rather, sea ice is made up of a mixture of open water, *pack ice* and *landfast ice*. Landfast ice, or fast ice, is frozen to the shore or it can be anchored to the sea floor in shallow, near shore environments. It swells with the tides but is otherwise immobile. Ice cover in landfast ice is generally continuous [Marshall, 2012]. In contras,t open-water ice floes, or pack ice, is discontinuous and highly mobile because it is statically unstable and breaks into fields of a mixture of open water and ice floes suitable for drifting, aptly called *drift ice*, that is then driven by ocean currents and wind stress [Leppäranta, 2011].

Drift ice is a peculiar geophysical medium with a large horizontal scale and a very small vertical scale, which translates into a very small aspect ratio (thickness vs. lateral extent) [Weiss, 2013]. Being thin, the direct Coriolis effect on the ice itself is rather weak in contrast to what happens to the atmosphere and ocean, because Coriolis force is proportional to mass [Wadhams, 2000]. It is granular, in the sense that ice floes are the elementary particles, and the drift takes place on the scale of floes and larger. The ice moves on the sea surface plane with no vertical velocity structure [Leppäranta, 2011]. Thus, sea ice drift can be treated as a two-dimensional problem.

Sea ice experiences a seasonal cycle of melting and refreezing, reaching a maximum extent in mid-March and a minimum around mid-September for the Arctic ocean. The ice cover is shaped by the seasonal insolation cycle and, in contrast to what happens in the

[1] [Wadhams, 2000]

Antarctic, also by the geometry of the Arctic basin (figure 1.1), which plays a role in limiting and defining the maximum ice extent.

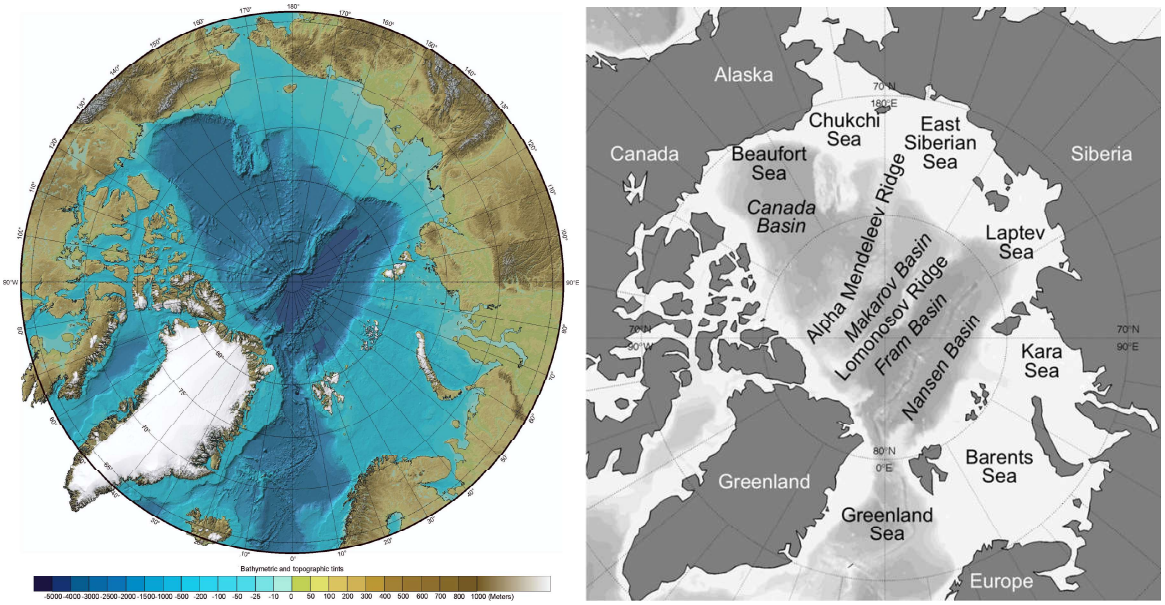

FIGURE 1.1: The geography of the Arctic basin (IBCAO,NOAA) and associated names

The ice experiences changes in extent during this seasonal cycle but also in thickness and strength, properties that in turn affect its dynamics. Sea ice thickens and strengthens with freezing through fall and winter by thermodynamic processes, growing from below through basal accretion or *aggradation*, and becomes thinner and weakens with melting during spring an summer [Marshall, 2012]. During winter, when the ice concentration (the fraction of the surface covered by ice) is near 100% and the mechanical strength of the ice is high, the surface stresses are propagated over distances comparable to the length scale of atmospheric weather systems [Weeks, 2010]

Autumn and winter are also the time of the year when new ice forms (known as first-year ice, FYI). The thermodynamic growth of sea ice is limited to a thickness of about 2 meters. Thicker ice develops through mechanical ridging under convergence, compression and overriding of ice floes, a process highly dependent on sea ice dynamics. Through the spring and summer a large fraction of FYI melts away or is advected to lower latitudes. That which survives the summer becomes multi-year ice (MYI). The thickest multi-year ice is a result of ice convergence against the Canadian Archipelago and Northern Greenland, where it piles up due to the prevalent wind forcing [Marshall, 2012].

The transition between the open ocean and sea ice is known as the marginal ice zone (MIZ). Depending on factors like wind direction and ocean currents, it may consist of anything from isolated, small and large ice floes drifting over a large area to a compact edge of small ice floes pressed together in front of solid pack ice. The MIZ is very dynamic due to the influence of the weather and rapid changes. Changes in its extent may take place over hours or days.

The circulation of sea ice is illustrated by its velocity field which can be decomposed into a predictable component, associated with the long-term average wind and ocean currents, and a random part associated with the short-term fluctuations in wind and currents [Thorndike, 1986] Put it otherwise, into a deterministic mean field and the random fluctuations from that mean [Weiss, 2013]. This approach suggests the existence of an Arctic General Circulation (AGC), represented by the deterministic part of the motion. The fluctuating part of the motion would be the result of atmospheric and oceanic turbulence.

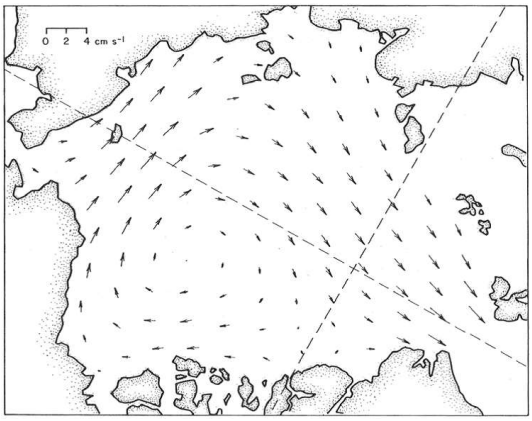

FIGURE 1.2: Sea ice drift main field from Thorndike and Colony, 1984

The first mean ice drift field, presented by Gordienko (1958) and based on the drift of ships and manned stations, was later revised by [Colony and Thorndike, 1984], adding large amounts of drift buoy data. Their analysis is summarized in figure 1.2, where the detailed structure of the Arctic dynamics main features became evident. Generally, the circulation of sea ice is highly variable on weekly to monthly time scales but is dominated, on average, by a clockwise motion pattern in the western Arctic, the *Beaufort Gyre*, and by a persistent southward flow, the *Transpolar Drift Stream* (figure 1.3), that exports approximately 10% of the area of the Arctic basin through the Fram Strait every year (ref). Such a general circulation, in the form of a transpolar current, was already postulated by Nansen on the basis that fragments of the "Jeannette", a ship that had sunk north of the New Siberian Islands, were found three years later on the south coast of Greenland [Weiss, 2013].

This mean field was then considered as the AGC, linked to the large-scale atmospheric circulation [Colony and Thorndike, 1984]. Packed ice that is entrained in the Beaufort Gyre can circulate through the Arctic basin for several years before being exported to the North Atlantic through Fram Strait and the East Greenland Current, and the channels of the Canadian Archipelago. The role of this circulation on the mass balance of Arctic sea ice, and so on its long-term evolution, is essential, especially through the sea ice export across Fram Strait [Kwok and Rothrock, 1999].

From that mass balance perspective, the amount of sea ice in the Arctic is dictated both by thermal and dynamical forcing. The Arctic Ocean loses ice by melt and by export, hence the interest in southward transport of ice through Fram Strait. Although some studies report that the MYI loss in the Arctic Basin during the first decade of this century has occurred mainly by melting [Kwok and Cunningham, 2010], the relative contribution of melt and export to the loss remains uncertain [Jeffries, 2013; Kwok and Untersteiner, 2011]. This unresolved question highlights the fact that the dynamics of sea ice are tightly coupled with

thermodynamics since, as we noted above, freezing strengthens and melting weakens the ice, while ice motion influences the further growth or melting of ice via transport, to higher or lower latitudes, and differential motion, that causes ridging or rifting [Marshall, 2012].

The dynamics of sea ice have been studied systematically since the times of the aforementioned Fridtjof Nansen and the *Fram* expedition to the Arctic he led between 1893 and 1896, during which he observed that his ship, trapped in ice, drifted with it consistently at 2% of the surface wind speed and at 20-40^o to the right of the surface wind direction [Leppäranta, 2011]. In a seminal paper inspired by the data collected in Nansen's expedition Ekman attributed this effect to a balance between the wind forcing, ice-water drag and the Coriolis acceleration [Ekman, 1902]. The Fram expedition provided the first-ever dataset on sea ice drift in relation to wind forcing and ocean currents and some authors consider that sea ice became part of modern geophysics after this pioneering work [Weeks, 2010].

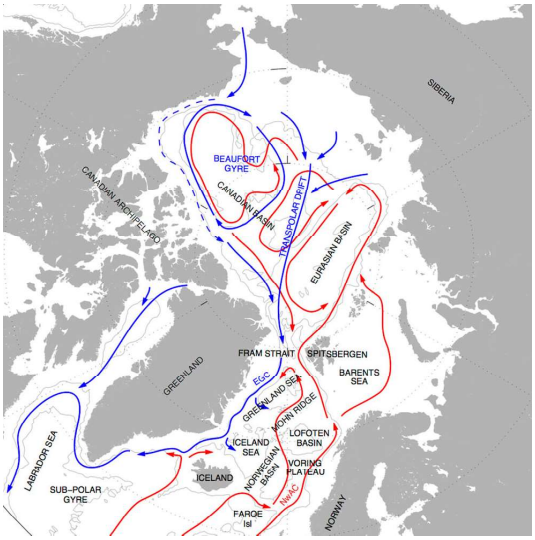

FIGURE 1.3: Schematic Arctic sea ice circulation (surface currents in blue, bottom currents in red)

The full ice drift problem includes three unknowns: ice state, ice velocity and ice stress. The system is closed according to equations for the conservation of ice, the conservation of momentum, and ice rheology. Ice is driven by winds and ocean currents and responds to forcing by its inertia, internal friction, and adjustment of its state field. The Coriolis effect slightly modifies ice movement [Leppäranta, 2011].

1.2 Sea ice drift estimation

Scientific interest in sea ice and how it moves arises in the first place from the problem that this barrier represents to sea navigation and offshore operations (e.g.fisheries) in high latitudes. Tightly connected with this issue are the effects of ice loads on fixed structures and ships. And with the development of commercial and industrial activities in the Arctic there is also and increasing interest in studying the transport of pollutants, specially oil spills.

But these issues being important, scientists are also interested in sea ice dynamics for other reasons. Arctic sea ice extent, largely influenced by ice drift, has a key role in the

cryospheric albedo effect and its associated feedbacks. The motion of sea ice is also important for analyses of parameters describing the interaction between ocean, sea ice and atmosphere, such as heat exchange or salinity transport [Linow et al, 2013]. And sea ice is closely related to the formation of deep water and, ultimately, the thermohaline circulation.

The scientific study of sea ice drift has essentially all been carried out during the last 100 years, with most of the effort concentrated on the period after 1950. After Nansen's pioneering expedition, observations and analysis of sea ice motion remained scarce during the first half of the twentieth century, mainly restricted to Soviet stations and manned camps deployed on the drifting pack ice as the former USSR was already interested at that time in developing the Northern Sea Route along the Siberian coast. When the Cold War started, geopolitical interest on the Arctic from both contending sides took over purely navigational issues and sea ice studies started gradually to proliferate [Weeks, 2010].

The first major western experiment specifically designed to study how sea ice moves and changes in response to the influence of the ocean and the atmosphere was the Arctic Ice Dynamics Joint Experiment (AIDJEX). The field program took place in 1975 and 1976 with the deployment of four manned camps and ice drifters with an automatic ARGOS positioning system on ice floes in the Beaufort Sea, and led to significant progress in the characterization and modeling of sea ice dynamics. Since then, the amount of data available from in situ measuremets has increased considerably. Another relevant example is the International Arctic Buoy Program (IABP), an effort that groups institutions from several countries and maintains since 1979 a network of automatic data buoys to monitor ice motion throughout the Arctic Ocean. In situ measurements provide very reliable data but the downside of this campaigns is their limited spatial resolution.

The use of airborne instrumentation to monitor sea ice had come of age prior to World War II and became common practice afterwards. That enlarged further the area of study and complement the results obtained by in situ measurements. Until the 1980s aircraft survey was the main method for a regular observation and charting of sea ice. But the advent of remote sensing of sea ice from satellites in the late 1970s has completely revolutionized the field, since this observational platform provides researchers with data covering a wide range of spatial and temporal scales. Regular monitoring of sea ice with passive microwave sensors on board orbiting satellites has been done continuously since 1979 and the data collected this way represent one of the longest Earth observation records from space. [Sandven et al., 2013] Nonetheless, data from other platforms and instruments such as airborne surveys and in situ measurements are still needed to assess the accuracy of the satellite observations. As a result of the combination of all these different techniques, sea ice is nowadays monitored with an unprecedented degree of detail. And that has led to relevant discoveries about Arctic processes.

1.3 The Arctic shifts to a new state

Until relatively recent times the seasonal cycle discussed above was thought to be remarkably consistent from year to year and in a near-steady state. But the satellite record has revealed a sharp decrease of the sea ice cover over the Arctic during the last decades, both for the annual maximum in mid-March and the annual minimum in mid-September (Figure1.4). The maximum has dropped from 16.2 million km^2 in 1980 to a record low of 14.5 million km^2 in 2016, and the minimum from 7.9 million km^2 in 1980 to 3.6 million km^2 in 2012, as reported by the National and Snow Data Center (NSIDC)

Over the past 30 years the average September ice extent has been declining at an astonishing rate of 13.4 per cent per decade relative to the 1981-2010 average (Figure 1.5). Trends are smaller during March (-2.6 per cent per decade), but are still decreasing at a statistically significant rate [NOAA 2016 Arctic Report]

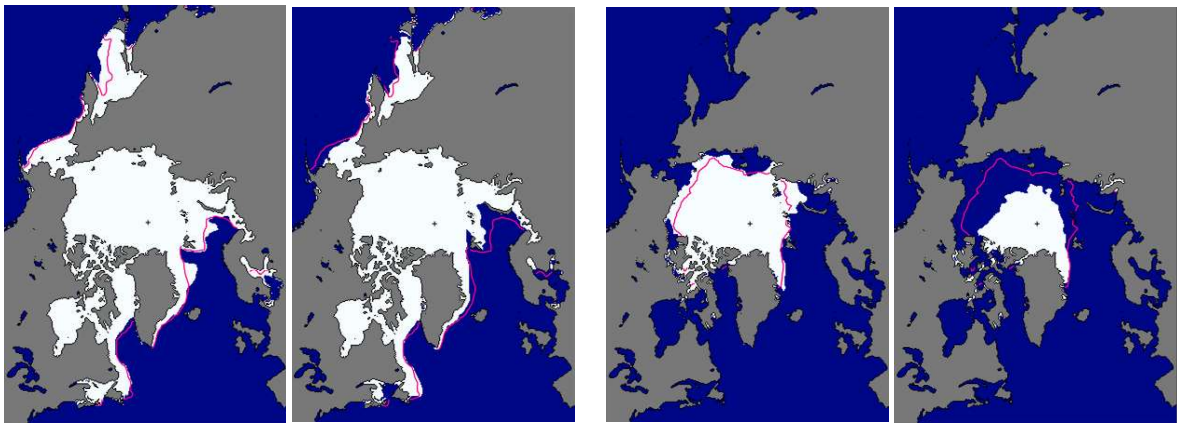

(A) March 1980 (B) March 2016 (C) September 1980 (D) September 2012

FIGURE 1.4: Evolution of maximum and minimum Arctic sea ice extent. The magenta line shows the 1981 to 2010 median extent.

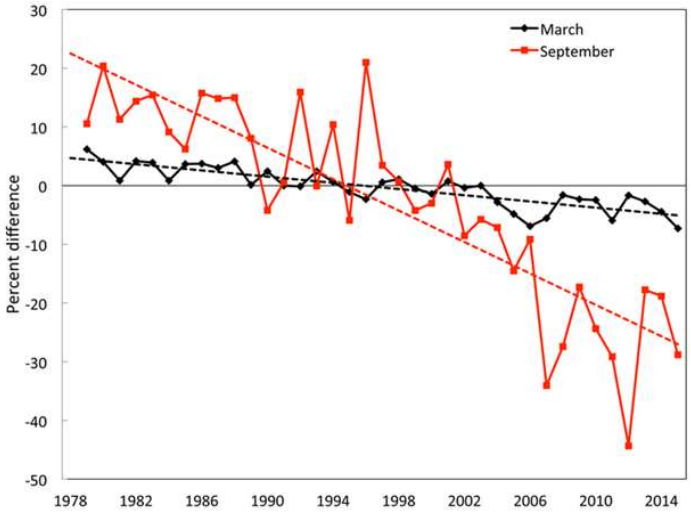

FIGURE 1.5: Time series of Northern Hemisphere sea ice extent anomalies

Sea-ice extent is declining faster than models predict. The observed rates of shrinking and thinning of sea ice in the Arctic Basin during the past three decades were greatly underestimated by the 2007 IPCC-AR4 climate models; indeed, none of the models could quantitatively explain the trends experienced in the Arctic [Kwok and Untersteiner, 2011] The recent CMIP5 studies have shown that climate models in general predict that the summer sea ice in the Arctic will disappear in this century, but there is large discrepancies between the models when this will happen [Stroeve et al., 2012]. This suggests that there are important processes that are nor adequately represented in the climate models (Sandven et al., 2013)

A less obvious but equally or even more relevant steady reduction in sea ice volume during the last 50 years has been reported by numerous researchers. Their studies were initially based on US Navy data of sea ice draft measured from submarines, and lately on remote sensing [Rothrock et al., 2008] The ice draft is the depth of the submerged portion of the floating ice observed by upward-looking sonars on submarines and is converted to thickness using Archimedes Principle and the densities of ice and seawater.

As it happened with the sea ice extent and the arrival of passive microwave measurements from satellites, the launch of ICESat (Ice Cloud Land Elevation Satellite) in 2003 and of CryoSat in 2012 have provided researchers with a nearly complete mapping of ice thickness from space, and the wealth and quality of that data has helped to confirm the previous observations [Kwok and Rothrock, 2009].

Besides, this average thinning is not homogeneous. During the period 1980-2012 the MYI cover has decreased from 62 to 42% cent and has been replaced by much thinner FYI. Age and thickness make the ice more resilient to atmospheric and oceanic forcing. Thinner ice is also more translucent, and a direct consequence is the already documented increase in biological primary productivity in the water below the ice and in previously ice-covered waters [Jeffries et al., 2013].

Sea ice thickness is relevant for its own drift because it determines ice strength and consequently internal ice stress. The thicker the ice, the stronger the stress. Or put it otherwise, the thicker the ice the more effectively it counteracts the wind stress. As the ice becomes thinner we can anticipate the opposite effect, that is, sea ice stresses will oppose less the wind (and oceanic) forcing in those areas experiencing decrease in thickness.

The shift to a younger, thinner ice cover is due to dynamic and thermodynamic processes but determining the relative contribution of each one of them to the whole remains a difficult research problem [Jeffries, 2013; Kwok and Untersteiner, 2011].

1.4 A linear regression model

However, in spite of all those fulfilled achievements by the remote sensing revolution, considerable observational uncertainties remain. In this thesis we try to contribute to one of those uncertainties.

Met Norway provides sea ice drift products derived from data obtained through several spaceborne platforms. The algorithms employed to construct such products are based on the technique known as *motion tracking* which consists in following the displacements of brightness temperature patterns observed from consecutive images of passive microwave satellite sensors [Bischof, 2000]. Similarly to other motion tracking applications in geosciences (e.g. sea surface currents, winds), sea ice motion vectors are computed by cross-correlation of pairs of satellite images [Lavergne et al., 2010]. Due to surface melting and a denser atmosphere, the latter being a direct consequence of its increased water vapour content, sea ice drift vectors cannot be retrieved reliably during summer from the satellite instruments and channels they are currently using, which results in noisy data [Lavergne, 2015]. Our contribution consists in an independent estimate of sea ice drift based, not on direct observations, but on a theoretical model. The hope is that MET Norway can make a more reliable drift estimate from a combination of their remote sensing estimate and our model.

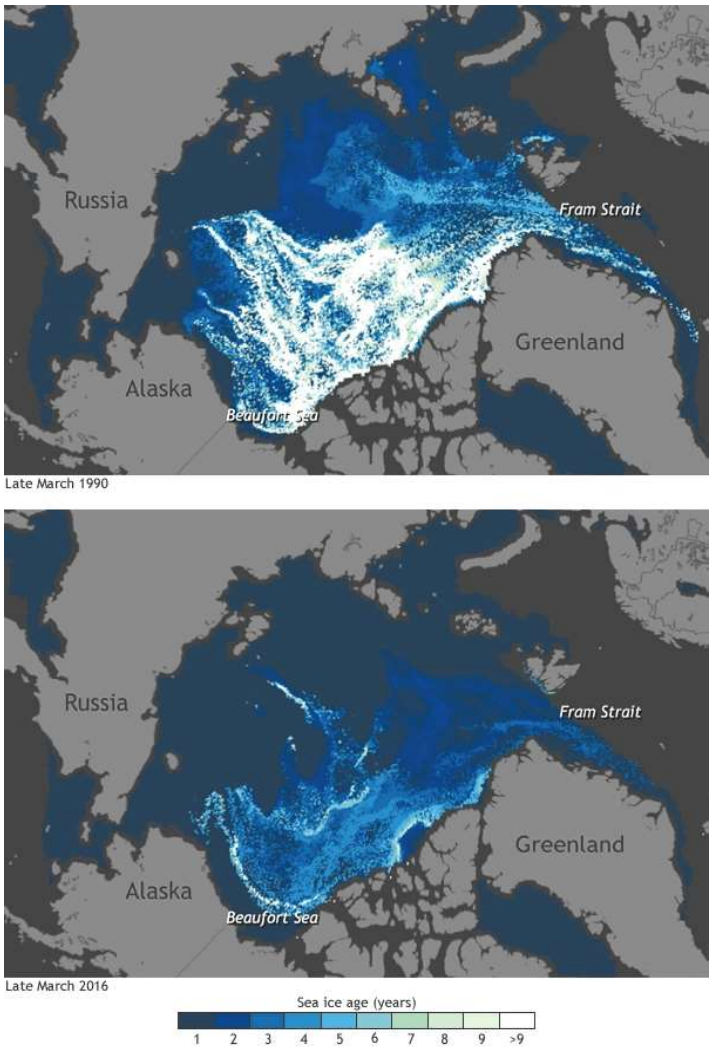

FIGURE 1.6: Evolution of sea ice age (thickness) 1990-2016

In what follows we outline the remainder of the content of this thesis.

We apply the two-dimensional equation of motion of sea ice to one simple drift regime known as free drift, the one that first attracted Nansen's attention, where internal ice stresses are neglected. The free drift problem results, under certain assumptions, in an algebraic equation with a linear solution of the form

$$\vec{u} = \vec{A}\vec{U_a} + \vec{U_w} + \vec{e} \tag{1.1}$$

We investigate the usefulness of this linear model for sea ice drift in order to predict the time evolving sea ice velocity $\vec{u}$ from time-evolving surface winds $\vec{U_a}$ and steady geostrophic ocean currents $\vec{U}$. We allow for a random noise term $\vec{e}$ that will helps us later on in estimating the validity of the model. The parameter $\vec{A}$ is a proportionality constant which also contains information about angular offsets. We apply the inverse theory [Wunsch, 1996; Menke, 2012] to solve this equation.

This relationship has already been used by other researchers in an inverse sense, that is, they have used sea ice drift and surface wind observations to solve for the parameter $\vec{A}$ and

the average sea currents $\vec{U_w}$. We however elaborate more on the otherwise limited assessment of the validity of the model. We achieve this by studying the structure of the residuals, or error of the estimate, by checking where they actually take on a Gaussian structure and are also free of autocorrelations, both requirements for true random noise. Besides we try to determine if the residuals are a function of the wind.

The results are assessed with respect to a priori assumptions. As stated above, the main objective is to provide MET Norway with good enough estimates of the uncertainty associated with this model. It is expected that it will help their operational estimates of Arctic Ocean sea ice drift velocities when making use of it in a forward sense. By that we refer to solve equation 1.1 for the sea ice drift velocity $\vec{u}$ from wind velocities $\vec{U_a}$ and the model parameters $\vec{A}$ and $\vec{U}$.

Data specifications and a detailed explanation of the applied methodology follows the theoretical explanation.

After that we present the results of our study in general, and then from a seasonal and decadal perspective, for each of the model parameters A and C and also for the coefficient of determination and the residuals. We elaborate on the statistical analysis of those residuals in order to evaluate how valid the model is to provide a theoretical estimate of sea ice drift.

We end up this thesis exposing the conclusions we have reached and what perspectives seem to await sea ice in the future.

Chapter 2

Theory

"Mathematics is the easiest bit in physics"

Pierre-Gilles de Gennes, "Les objets fragiles"
(1991 Physics Nobel Prize laureate)

2.1 Equation of motion

The motion of sea ice takes place in a three-dimensional world, but it can be treated as a two-dimensional phenomenon on the sea surface. After integrating the three-dimensional equation through the thickness of the ice [Leppäranta, 2011] a two-dimensional equation of motion of sea ice on the sea surface plane results

$$h\rho\left(\frac{\partial\vec{u}}{\partial t}+\vec{u}\cdot\nabla\vec{u}+f\vec{k}\times\vec{u}\right)=\nabla\cdot\vec{\sigma}+\vec{\tau}_a+\vec{\tau}_w-h\rho g\nabla\vec{\eta}-h\nabla p_a \tag{2.1}$$

where h is the sea ice thickness, ρ is the sea ice density, $\vec{u}$ is the sea ice velocity, $\nabla\cdot\vec{\sigma}$ is the internal sea ice stress, $\vec{\tau}_a$ is the stress of the wind, $\vec{\tau}_w$ is the stress of the water, g is the gravitational acceleration, η is the sea level elevation and p_a is the atmospheric pressure.

As is common practice in ocean dynamics the full Coriolis acceleration is reduced to its vertical component, $f\vec{k}\times\vec{u}$, where $f=2\Omega\sin\phi$ is the *Coriolis parameter*, $\Omega=7.29\cdot10^{-5}\,s^{-1}$ is the angular velocity of the Earth, and ϕ is the latitude.

2.1.1 Scaling and dimensional analysis

The ice variables in the momentum equation are thickness, velocity, and strength, all of which depend on time and space. Sea ice strength relates directly to its internal stress, and can be defined as the nature and magnitude of stress needed to make the ice fracture [Wadhams, 2000]. The magnitudes of their scales are now rather well known from the long-term database built up over the years. Table 2.1 summarizes those values.

Dimensional analysis of the momentum equation is performed based on the typical scales of these variables and the results are shown in table 2.2, from where it can be inferred that the governing terms are wind and water stresses, and internal friction [Leppäranta, 2011] (figure 2.1).

The internal friction of ice is the most difficult term because there are still unsolved phenomenological problems. However, the significance of the internal friction is limited to

compact ice fields; in open ice fields this term will be ignored as the basic statement of the free drift case.

Coriolis acceleration and sea surface tilt are an order of magnitude smaller than the air and water stresses, and the local and advective accelerations are smaller still (table 2.2). The air pressure term is minor and will be excluded from further analysis.

	Typical	Low	High
Thickness, H	1 m	0.1 m	10 m
Velocity, U	0.1 m/s	0	1 m/s
Strength, P	10 kPa	0	100 kPa
Time, T	10^5 s	10^3 s	∞
Length, L	100 km	10 km	1000 km

TABLE 2.1: Typical and extreme values of sea ice variables [Leppäranta, 2011]

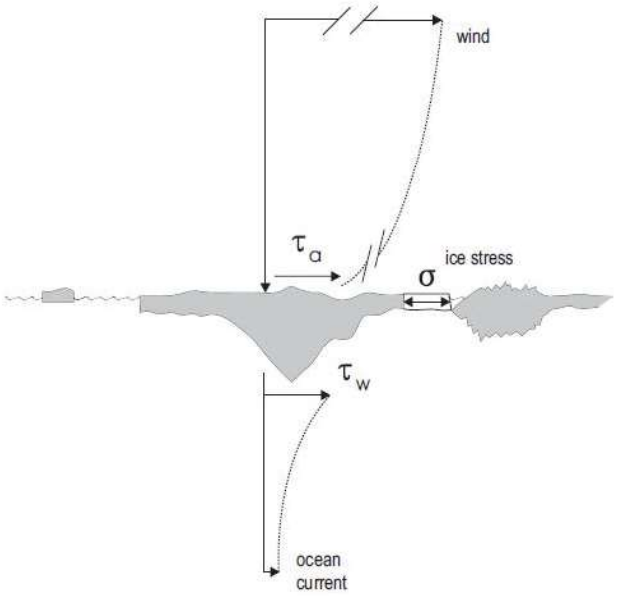

FIGURE 2.1: Schematic representation of the sea ice drift problem

2.2 Free drift

Free drift is defined as the drift of sea ice in the absence of internal ice stresses. The situation has been known from the times of the *Fram* expedition. The experience gained in that expedition was determinant in finding the solution for this particular sea ice drift regime.

To solve for the full ice drift problem three unknowns, namely ice state, ice velocity and ice stress, should be characterized from a closed system consisting of the equations for the conservation of ice, the conservation of momentum, and the ice rheology. The free drift solution of sea ice dynamics it is only based on the momentum equation. Because there is no internal stress the ice rheology is not necessary, and the ice conservation law it

Term	Scale	Value
Local acceleration	$\rho HU/T$	10^{-3}
Advective acceleration	$\rho hU^2/L$	10^{-4}
Coriolis acceleration	ρHfU	10^{-2}
Internal friction	PH/L	10^{-1}
Wind stress	$\rho_a C_a U_{ag}^2$	10^{-1}
Water stress	$\rho_w C_w \lvert U_{wg} - U\rvert^2$	10^{-1}
Sea surface tilt	$\rho H f U_{wg}$	10^{-2}
Air pressure	$H\rho_a f U_a$	10^{-3}

TABLE 2.2: Scaling of the terms of the momentum equation of drift ice. In addition of the typical values from table 2.1 the following values have also been used: U_{ag} = 15 m/s, U_{wg} = 0.05 m/s [Leppäranta, 2011]

is not normally solved [Leppäranta, 2011]. The free drift case is a good approximation for individual, separate ice floes and for ice fields with small compactness.

The following simplifications from the momentum equation of sea ice drift (equation 2.1) are made:

- Internal friction, $\nabla \cdot \vec{\sigma}$, is neglected as the basic assumption of ice drift
- The air pressure gradient is in general a minor term in sea ice drift
- The local and advective acceleration are also small terms

as shown by scale analysis for those last three components (section 2.2).

For this steady state an algebraic equation results:

$$h\rho f\vec{u} = \vec{\tau}_a + \vec{\tau}_w - h\rho g\nabla\vec{\eta} \tag{2.2}$$

Because we assume the ocean currents ($\vec{U_w}$) to be geostrophic in this drift regime, the sea surface tilt can be written in terms of the geostrophic current:

$$f\vec{k} \times \vec{U}_{wg} = -g\nabla\vec{\eta} \tag{2.3}$$

and then combines with the Coriolis acceleration to produce a single term. The algebraic equation then ends up being:

$$\vec{\tau}_a + \vec{\tau}_w - h\rho f(\vec{U}_{wg} - \vec{u}) = 0 \tag{2.4}$$

or in a more compact form

$$\vec{\tau}_a + \vec{\tau}_w = Cor + T \tag{2.5}$$

where $Cor + T$ is the single term that represents together the Coriolis and sea surface tilt terms.

The drag force exerted by a fluid on a surface is typically made to be proportional to the square of the fluid speed relative to that surface, U,

$$\tau = \rho C U^2 \tag{2.6}$$

where ρ is the density of the fluid and C is the drag coefficient, a constant of proportionality linking fluid speed to stress exerted on the surface, and that it is a function of the roughness of the surface. [Wadhams, 2000]

There are two different kinds of sea ice roughness: the small scale roughness of the top surface of undeformed ice floes which relates to *skin friction drag*, and the large scale roughness which results from the ice deformation due to convergence, compression and overriding of ice floes. This creates vertical structures which protrude into the air and water flows and causes *form drag*.

In planetary boundary layers the Coriolis effect causes the flow to turn, and therefore a second stress parameter, the turning or Ekaman angle, is required between the flow and the surface stress. By using this quadratic drag law the wind stress on the sea ice is expressed in general form as

$$\vec{\tau}_a = \rho_a C_a |U_a| e^{i\theta_a} \vec{U}_a \tag{2.7}$$

where ρ_a is the air density, C_a is the air drag coefficient, θ_a is the boundary-layer turning angle in air and $\vec{U}_a$ is the wind velocity. To determine the wind stress exactly the wind velocity relative to the ice should be $(\vec{U}_a - \vec{u})$, where $\vec{u}$ is the ice velocity, instead of only $\vec{U}_a$. But since $\vec{U}_a >> \vec{u}$ the approximation used is good enough.

As it was done before with the sea surface tilt the water stress on the sea ice can be written in terms of the geostrophic current :

$$\vec{\tau}_w = \rho_w C_w |U_{wg} - u| e^{i\theta_w} (\vec{U}_{wg} - \vec{u}) \tag{2.8}$$

where ρ_w is the water density, C_w is the water drag coefficient, θ_w is the boundary-layer turning angle in water, $\vec{U}_{wg}$ is the geostrophic water velocity and $\vec{u}$ is again the ice velocity. Now $\vec{U}_{wg}$ and $\vec{u}$ are of similar magnitude and the water velocity relative to the sea ice depends on both. It is just as often the case that surface water is exerting a drag to slow down an ice floe being moved by the wind as it is that a strong current is trying to accelerate a floe.

After replacing the stress terms into equation 2.4 we end up with the equation of momentum for the free drift case by components.

$$\rho_a C_a |U_a| e^{i\theta_a} \vec{U}_a + \rho_w C_w |U_{wg} - u| e^{i\theta_w} (\vec{U}_{wg} - \vec{u}) - h\rho f (\vec{U}_{wg} - \vec{u}) = 0 \tag{2.9}$$

The mathematical core of this thesis is based in a simplified solution to this equation, as it will be explained in the following section.

2.2.1 Thorndike and Colony, 1982

In this seminal paper [[ref]] the authors based their analysis of sea ice drift on the free drift solution (the complex non-linear equation 2.9 or, alternatively, its compact version 2.5) for which they propose two limiting cases.

Small U_a	Large U_a
$Cor + T \gg \vec{\tau}_w$	$Cor + T \ll \vec{\tau}_w$
$\tau_a + Cor + T = 0$	$\tau_a + \tau_w = 0$
$u = \lvert A' \rvert \lvert U_a \rvert U_a e^{-i\theta'} + U_{wg}$	$u = \lvert A \rvert U_a e^{-i\theta} + U_{wg}$

TABLE 2.3: Solutions to limiting cases

The non-linear effects are only felt for small values of $|U_a|$, where the theory predicts that $|u|$ should increase as $|U_a|^2$ (first column in table 2.3). For large values of $|U_a|$ the response is linear as $|u|$ is proportionals to $|U_a|$ (second column in table 2.3). The nearly linear behaviour in equation 2.9 is a consequence of the arrangement of vector forces acting on drifting sea ice (figure 2.2). Except at low wind speeds, the air and water stress roughly balance each other.

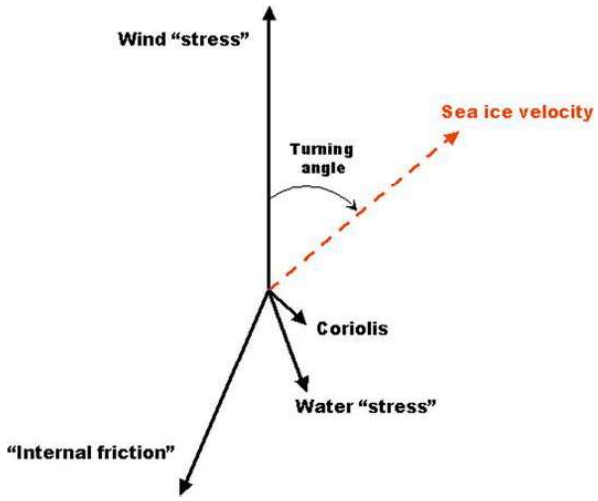

FIGURE 2.2: Schematic diagram of forces acting on drifting sea ice. The "internal friction" vector is neglected in the free drift regime.

As the objective of this thesis is to evaluate the utility of a linear model of sea ice drift, we focus on the second limiting case. However, the first one is not completely ignored and it will come up later on while analysing the validity of the model.

For a large U_a the Coriolis and the sea surface tilt terms are small with respect to the water stress and then the solution to equation 2.9 is

$$\vec{u} = A\vec{U}_a + \vec{U}_{wg} \tag{2.10}$$

A is a complex coefficient

$$A = |A|e^{-i\theta} \tag{2.11}$$

where $|A|$ is the wind scaling factor, also known as the Nansen number [Leppäranta, 2011; Weiss, 2013],

$$|A| = \sqrt{\frac{\rho_a C_a}{\rho_w C_w}} \tag{2.12}$$

and

$$\theta = \theta_w - \theta_a \tag{2.13}$$

is the deviation angle from the wind-driven ice drift direction to the wind direction. θ_w is positive in the Northern Hemisphere, and as $\theta_a = 0$ for the surface wind, we have $\theta = \theta_w > 0$ [Leppäranta, 2011]. By convention, a positive angle is generated by counter-clockwise rotation (in the Northern Hemisphere). But, as the rule of thumb states [Nansen, 1902], the drift of sea ice is to the right of the direction of the wind (again, in the Northern Hemisphere) in clear contrast with the way θ is defined above. As this definition seems counterintuitive

the discrepancy is solved by placing a minus sign before θ in equation 2.11 and making rotation clockwise and the angle negative.

The theory behind this linear solution is best applicable in summer conditions, when there are free paths between floes and open-water areas do not freeze [Leppäranta, 2011].

As stated above, at low wind speeds the straight free drift model is questionable, since the stratification of air and water may play a major role [Leppäranta, 2011]. When the wind speed is less than 2 m/s there is no longer any clear connection between ice motion and wind [Rossby and Montgomery, 1935], since the local wind is overcome by the wind field over a larger area and by ocean currents as well.

2.3 Finding $\vec{A}$ and $\vec{U}_w$: inverse modelling

The resulting equation $\vec{u} = A\vec{U}_a + \vec{U}_{wg}$ represents a linear model of sea ice drift under ice stress-free and moderate to strong wind conditions. Despite its apparent simplicity, if we are able to solve it and make reliable estimates of the model parameters $\vec{A}$ and $\vec{U_w}$, we will be in a good position to make trustworthy estimates of sea ice drift in the future, based on those same parameters and wind velocity measurements.

2.3.1 Inverse problem

Inverse theory is an organized set of mathematical techniques and methods used for reducing *data* to obtain *knowledge* about the world's *physical properties* as inferences drawn from observations [Menke, 2012].

While *knowledge* can take many forms, inverse theory deals with the sort that can be represented numerically. And depending on how these "numbers" are represented, the *physical properties* we're trying to get insight from can be classified into two general categories: those that can be described by *discrete parameters* and those that must be described by *continuous functions*. Inverse theory employs a different set of mathematical methods for each one: the *theory of matrix equations* for discrete parameters and the *theory of integral equations* for continuous functions.

In spite of dealing in our study with continuous, random variables we will apply to the data the techniques employed in the discrete case due to the convenient fact that continuous functions can be studied by the discrete version of inverse theory as long as they are adequately approximated by a finite number of discrete parameters. In this way, a continuous variable can be represented by its value at a finite number of closely spaced points.

The data in inverse theory are necessarily discrete since inverse theory is concerned with deducing knowledge from observational data, which is basically a tabulation of measurements that always have a discrete nature.

Another advantage of this approach is that the discrete version of the inverse theory relies mainly on the theory of vectors and matrices (linear algebra) rather than on the somewhat more complicated theory of continuous functions and operators.

2.3.2 How does this work?

The basic statement of an inverse problem, which in itself allows for the inference process, is that the *model parameters* (m) and the *data* (d) are somehow related, in a implicit, functional relationship called *quantitative model*,

$$d = f(m) \tag{2.14}$$

In inverse theory we systematically analyse the data to infer the values of the model parameters. Their estimates (simply a set of numerical values) have to be meaningful, that is, they have to capture the essential character of the process modelled. Besides, they also constitute the simplest and most useful kind of solution to the inverse problem. On the other hand, they can sometimes be misleading: estimates in themselves give no insight into the quality of the solution.

The model usually takes the form of one or more explicit equations that summarize what is known about how the measured data and the unknown model parameters are related.

The function, *f*, can be arbitrarily complicated. However, in very many important cases it is either linear or can be approximated as linear, and those cases happen to be the simplest and best-understood inverse problems. Under these circumstances the function results in a one degree polynomial, with an certain number of model parameters (M), which constitutes the general form of the linear inverse problem

$$d_i = G_{i1}m_1 + G_{i2}m_2 + ... + G_{iM}m_M \tag{2.15}$$

where d_i are the data (dependent variable), G are the coefficients and m_i are the parameters (independent variables) of the polynomial.

If we itemise for N data elements we get N linear equations

$$\begin{aligned} d_1 &= G_{11}m_1 + G_{12}m_2 + ... + G_{1M}m_M \\ d_2 &= G_{21}m_1 + G_{22}m_2 + ... + G_{2M}m_M \\ &\vdots \\ d_N &= G_{N1}m_1 + G_{N2}m_2 + ... + G_{NM}m_M \end{aligned}$$

and that can be conveniently represented in matrix form as

$$\begin{bmatrix} d_1 \\ d_2 \\ d_3 \\ \vdots \\ d_N \end{bmatrix} = \begin{bmatrix} G_{11} & G_{12} & \cdots & G_{1M} \\ G_{21} & G_{22} & \cdots & G_{2M} \\ \vdots & \vdots & \ddots & \vdots \\ G_{N1} & G_{N2} & \cdots & G_{NM} \end{bmatrix} \begin{bmatrix} m_1 \\ m_2 \\ m_3 \\ \vdots \\ m_M \end{bmatrix}$$

or in a more compact form

$$d = Gm \tag{2.16}$$

where *d* and *m* are the *data* and *model parameters* vectors. The matrix *G* is the *data kernel* that contains the coefficients of the linear relationship. It relates N data to M model parameters and so its dimensions are N $\times$ M.

This equation forms the foundation of the study of discrete inverse theory, which main purpose is to solve it, or "invert" it, to provide estimates of the model parameters, m^{est}.

Once those parameters have been estimated the equation can also be solve in a "forward" sense to make predictions of the data.

$$d^{est} = Gm^{est} \tag{2.17}$$

In most typical data analysis cases N $\neq$ M; in fact, usually N $\gg$ M. Because we're dealing with much more data than model parameters the problem is said to be *overdetermined*; there is too much information contained in the equation $d = Gm$ for it to posses an exact solution. Stated otherwise, the equation cannot be satisfied for every data point because of measurement noise and, therefore a solution for which the predicted data matches the observed data, $d^{est} = d^{obs}$, (every individual error equals zero) does not exist. So then

$$d^{obs} \simeq Gm^{est} \tag{2.18}$$

or more precisely

$$d^{obs} = Gm^{est} + e \tag{2.19}$$

where e is the random error.

The alternative is to look for the "best" approximate solution among the many possible ones, the one with a model parameters estimate that allows for the smallest average difference (smallest average error) between the predicted data and the observed data ($d^{est} \simeq d^{obs}$).

Combining equations 2.17 and 2.19 an individual prediction error is defined for each observation:

$$e_i = d_i^{obs} - d_i^{est} = d_i^{obs} - G_i m^{est} \tag{2.20}$$

2.3.3 Least squares for a straight line

If we restrict the model to a single independent variable, the original polynomial reduces to the equation of a line. Our inverse problem becomes then the problem of fitting a straight line to data.

$$d_i = m_1 x_i + m_2 \tag{2.21}$$

where m_1 and m_2 are the unknown parameters.

For N data elements we get N linear equations

$$\begin{aligned} d_1 &= m_1 x_1 + m_2 \\ d_2 &= m_1 x_2 + m_2 \\ &\vdots \\ d_N &= m_1 x_N + m_2 \end{aligned}$$

or in matrix form

$$\begin{bmatrix} d_1 \\ d_2 \\ d_3 \\ \vdots \\ d_N \end{bmatrix} = \begin{bmatrix} 1 & x_1 \\ 1 & x_2 \\ \vdots & \vdots \\ 1 & x_N \end{bmatrix} \begin{bmatrix} m_1 \\ m_2 \end{bmatrix}$$

and again in the general expression for the inverse problem.

$$d = Gm \tag{2.22}$$

This elementary inverse problem illustrates the basic procedure applied in this technique to solve for it.

The "best" approximate solution is the one with a model parameters estimate (slope and intercept) that leads to the smallest overall error, E, defined as the sum of the squares of the individual errors or least squares

$$E = \sum_{n=1}^{N} e_i^2 \tag{2.23}$$

We look for the minimum error by setting the derivatives of E with respect to the model parameters to zero, and solving the resulting equations.

Least squares can be extended to the general linear inverse problem. The total error is now defined as

$$E = e^T e = (d - Gm)^T (d - Gm) \tag{2.24}$$

The resulting least squares solution to the inverse problem $d = Gm$ is then

$$m^{est} = [G^T G]^{-1} G^T d^{obs} \tag{2.25}$$

The full computation can be find in Appendix **??**.

2.3.4 The residuals

That solution is just one of many but we choose this one and no other because it is the best estimation possible of the model parameters according to the criteria of least squares. It is the model that better approximates the data. But because it is an approximation we end up with a bunch of error estimates or residuals of different magnitude. [[They are in fact the same individual errors computed with equation 2.20 that we have minimised with the least squares approach.]] Those residuals contain information about aspects of the process that are not reproduced by the model plus pure measurement errors. They will enable us to make statements about how large and how frequent are the effects not taken into account or captured by the model like internal ice stresses, variable currents and so on [Thorndike and Colony, 1982]. We analyse those residuals further on to asses the validity of the model. To achieve that we need them to be random noise: to have Gaussian structure and to be uncorrelated.

To obtain the residuals for the inverse problem we proceed as per equation 2.20 but this time for the whole data set instead of for each observation.

$$e = d^{obs} - Gm^{est} \tag{2.26}$$

where now e, d^{obs} and G represent matrices

Substituting m^{est} for the least squares solution (equation 2.25) we obtain

$$e = d^{obs} - G[G^T G]^{-1} G^T d^{obs} \tag{2.27}$$

The residuals for the inverse problem [Wunsch, 1996] are then computed as follows

$$e = (I - G[G^T G]^{-1} G^T) d^{obs} \tag{2.28}$$

Chapter 3

Data and methods

"When you copy from one author, it's plagiarism; when you copy from many, it's research"

Wilson Mizner

3.1 Data

3.1.1 Sea ice drift

The winter dataset is derived from passive microwave analyses by Ron Kwok at NASA's Jet Propulsion Laboratory and covers the period from October 1978 to September 2004. The generation frequency was one file every two days. Data is organized on a grid of 47*57=2116 points.

The seasonal analysis is performed on an ice data product by MET Norway, also from passive microwave analyses, that covers the period October 2012 to September 2015. The generation frequency was one file every two days. Data is organized on a grid of 177*119=21063 point.

3.1.2 Wind

We make use of re-analysed surface winds provided by ECMWF for the same periods shown above for the ice data. The generation frequency was again one file very two days. Data is displayed on a grid of 47*57=2116 points to match the winter ice dataset and on an grid of 177*119=21063 points to match the full-year one.

3.1.3 Sea Surface Height

We use re-analysed computer modelled values of Sea Surface Height generated by FOAM (Fast Ocean Atmosphere Model) for calculating the geostrophic velocities. The values are averaged for the period 1993-2002, and rotated and interpolated to match the 47*57 grid.

3.2 Methods

3.2.1 Two-dimensional motion using complex variables

The use of complex variables techniques is very convenient for the planetary boundary layer velocities because of rotational effects [Leppäranta, 2011]. We will perform our time series

analysis of the two-dimensional velocity vectors using complex variables. That implies denoting them as scalar variables, with real and imaginary components oriented along the x and y axes, respectively. As an example, ice velocity is expressed as $u = u_1 + iu_2$, where $i = \sqrt{-1}$. For a complex variable u, the magnitude or *modulus* is $\sqrt{u\bar{u}} = \sqrt{{u_1}^2 + {u_2}^2}$, where $\bar{u} = u_1 - iu_2$ is the complex conjugate of u. The direction or *argument* (the anticlockwise angle measured from the x axis) of u is denoted as *arg* u. Alternatively we can write as $u = |u|e^{i\theta}$, where $|u|$ is again the *modulus*, and θ is the anticlockwise angle.

In least squares analysis with complex variables the previous definition of the total error (2.24) is now defined as

$$E = e^H e = (d - Gm)^H (d - Gm) \tag{3.1}$$

where H stands for Hermitian, which is the transpose of the complex conjugate. Hence, the resulting solution is now

$$m^{est} = [G^H G]^{-1} G^H d^{obs} \tag{3.2}$$

and the equation to compute the residuals is

$$e = (I - G[G^H G]^{-1} G^H) d^{obs} \tag{3.3}$$

A complex number can be decomposed into a magnitude and an angle or the real (x) and imaginary (y) components. Because all data used in this thesis are represented in a two-dimensional polar stereographic projection we will refer to complex numbers by components. The real component represents displacements on the x axis and the imaginary component represents displacements in the y axis. To avoid confusion we will refer henceforth to them as the "x" and "y" components, respectively.

3.2.2 Solving our inverse problem: A and U_w

We invert for the model parameters A and U_w for every grid point on both sea ice drift and wind time series according to the adapted solution (equation 3.2), after transforming the variables to complex ones. The regressions are performed for every year and the results are then averaged. We choose a minimum number of days (20 for the winter, 10 for the summer) on which to do the regression to avoid outliers and provide robustness to our results.

The resulting matrix from the inversion contains the model parameters A and U_w that represent the wind scaling factor and the average geostrophic sea currents, respectively. A is then decomposed into its magnitude and direction, and plotted as filled contours. U_w is plotted in vector form as per its x and y components.

However, as the model is not the exact solution we need to assess its reliability through the analysis of the residuals or estimation of the error; we do that in order to evaluate by how much the model differs from observations.

3.2.3 The residuals

The complex residuals resulting from the least squares regressions performed to solve for the model parameters are computed according to equation 3.3, again at every grid point and on the same ice drift and wind complex time series that produced A and U_w. They are split into their constituent components and then quantified by their respective RMS (3.2.4). The plotting is also done by components. Besides, they are employed as the basis for the

normality and correlation tests performed, also by components, to asses whether or not they are random noise.

3.2.4 Assessing the validity of the model

Model validation is possibly the most important step in the model building sequence. To assess the validity of the model we need to quantify the extent to which the model fits the data. The quality or goodness of a linear regression fit is typically assessed using two related quantities: the Root of the Mean of the Squares (RMS) of the residuals and the R^2 statistic.

RMS is the most commonly-used measure to represent the residuals in the regression setting. It is considered an absolute measure of the lack of fit of the model and is measured in units of the dependent variable. The smaller the RMS of the residuals, the smaller the error of the estimate and, therefore, the better the fit.

R^2 provides an alternative measure of fit, in the form of the proportion of the variance explained. It is a measure of the linear relationship between the dependent and independent variables, it always takes on a value between 0 and 1, and is independent of the scale of the dependent variable.

The analysis of the residuals will be our main tool for model validation. We will make use of R^2 to analyse the proportion of variance of sea ice drift explained by the wind.

3.2.5 On the statistical analysis of the residuals

Our univariate inverse model is one method of many for modelling a process. Process modelling is defined as the concise description of the total variation in one quantity (the dependant variable; in our problem, the observed sea ice drift data, d^{obs}) by partitioning it into

- a deterministic component, given by a mathematical function that relates the dependant variable (d^{obs}) to the independent one (the wind data, G) through some parameters (m), and
- a random component (error, e) that is assumed to follow a particular probability distribution.

The mathematical expression for the modelling process is

$$d^{obs} = f(G, m) + e \tag{3.4}$$

We bring in the process modelling perspective to highlight the dichotomy between the deterministic structure of the data and its random variability, already implicit in the description of the inverse theory, but with important implications not discussed then about the validity of the model. There we focused on deterministic aspects. Here we emphasize on the random component of the relationship.

The data (d^{obs}) will vary deterministically according to the equation (AG + c) except for a small amount of random error (e). This random (measurement + modeling) error constitute an intrinsic part of the model itself, and it is in fact what makes the relationship between both variables a "statistical" one rather than purely deterministic. The reason behind this is that the functional relationship holds only on average, not for each data point (it does not satisfy every single point).

Like the parameters in the mathematical function, the random errors are unknown. They are simply the difference between the data and the mathematical function and cannot be characterized individually.

Underlying assumptions for process modelling

Implicit assumptions are inherent to any process modelling and it is important to understand what they are and comply with them because otherwise the validity of the model would be in question.

The random errors from different types of processes could be described by any one of a wide range of different probability distributions. However, with most process modelling methods, inferences about the process are based on the idea that the random errors are drawn from a normal distribution. One reason this is done is because the normal distribution often describes the actual distribution of the random errors in real world processes reasonably well. The normal distribution is also used because the mathematical theory behind it is well developed. If it turns out that the random errors in the process are not normally distributed, then any inferences made about the process may be incorrect.

Besides normally distributed, adjacent residuals should not be correlated with each other, that is, random errors are independent from one to the next. If the errors are not independent, then the estimate of the error standard deviation will be biased, potentially leading to improper inferences about the process.

The fulfilment of these residuals assumptions guarantees their true randomness. Non-randomness would imply that the deterministic part of the model is not fully capturing some explanatory information of the process modelled that would instead be registered by the residuals. We conclude then that to assess the validity of our statistical model we have to prove that the residuals resulting from the application of the inverse theory follow a normal (Gaussian) probability distribution and that they are free of correlations.

3.2.6 Normality tests

The importance of the normal distribution is undeniable since, as we have seen, it is an underlying assumption of many statistical procedures including linear regression analysis. If the normality assumption is violated, interpretation and inferences may not be reliable or valid. Therefore it is important to check for this assumption before proceeding with any relevant statistical method. There are two common ways to check the normality assumption: graphical means and formal normality tests. According to most authors [e.g. Razali et Wah, 2011] and statistics textbooks, the primary tool for assessing normality in most process modeling applications is graphical analysis.

But in our study in particular the graphical approach is not very practical because we are dealing with thousands of grid points. For that reason we base our statistical analysis of the residuals on two of the most widely used statistical tests for univariate normality.

Anderson-Darling test

The Anderson-Darling test assesses whether a given sample of data is drawn from a given probability distribution by comparing the cumulative distribution function of the data with the cumulative distribution function of a theoretical distribution to see if there is a good

agreement between them. The statistic A^2 is based on a squared measure of discrepancy between the hypothesized and the data distributions [Razali and Wah, 2011].

The test establishes as null hypothesis that the data comes from a given distribution. It also makes use of the empirical distribution in calculating critical values, which has the advantage of allowing for a more sensitive test. The null hypothesis is rejected if the test statistic is greater than the critical value. In spite of not being specifically designed to check for normality of data, when applied for a normal distribution it has proved to be one of the most powerful tools for that purpose [Razali and Wah, 2011].

This test is applied to check for normality with a statistical software program that computes both the statistic and the relevant critical values for different statistical significance levels. Instead of directly comparing the statistic and the critical value to asses for normality we take the ratio between the two for a certain statistical significance level (we choose α = 0.05). The data is assumed to be normally distributed (the null hypothesis is not rejected) if the value of the ratio is below one, and not normally distributed (the null hypothesis is rejected) if the value is above one.

Shapiro-Wilk test

The Shapiro-Wilk statistical test is specifically designed to determine whether a random sample comes from a normal distribution. The test statistic, W, is obtained by dividing the square of an appropriate linear combination of the sample order statistics by the usual symmetric estimate of variance. [Shapiro and Wilk, 1965]. The null hypothesis of this test is that the data is normally distributed. If the p-value for the hypothesis test is smaller than the chosen significance level (α = 0.05), then the null hypothesis is rejected.

The statistical software employed provides both the test statistic W and the p-value for the hypothesis test. Theoretically the value of W lies between 0 and 1. Small values of W lead to rejection of the null hypothesis whereas a value of one indicates normality of the data [Razali and Wah, 2011]. After practising with the software function we have noticed that W values are always very close to one when the p-value is bigger than α (the null hypothesis is not rejected). As the p-value becomes smaller than α so does W (and the null hypothesis is rejected). But even for p-values several orders of magnitude smaller than α, W doesn't get much smaller than 0.85-0.90. From this we interpret that any W value slightly below one will result in rejection of the null hypothesis.

3.2.7 Autocorrelation tests

Autocorrelation function

The autocorrelation function is a correlation coefficient that determines the degree of correlation between two values of the same variable at two consecutive instants in time. When used to detect non-randomness, it is usually only the first (lag 1) autocorrelation that is of interest.

Durbin-Watson test

The Durbin-Watson is a statistical test to check for autocorrelation in residuals from an ordinary least-squares regression analysis. It tests the null hypothesis that the residuals are not autocorrelated against the alternative hypothesis that the residuals follow an AR1 process (first-order autoregressive process). The Durbin-Watson statistic ranges in value from 0 to

4. A value near 2 indicates non autocorrelation; a value towards 0 indicates positive autocorrelation; a value towards 4 indicates negative autocorrelation. Once the statistic has been obtained it has to be compared with tabulated critical values.

Exact critical values of the Durbin-Watson statistic are not tabulated. Instead, upper and lower bounds for the critical values have been established, and values that fall in between are considered inconclusive. Typically, tabulated bounds are used to test the hypothesis of zero autocorrelation against the alternative of positive first-order autocorrelation, since positive autocorrelation is seen much more frequently in practice than negative autocorrelation. Taking into account the amount of data and the number of model parameters, as prescribed when looking for the tabulated critical values, we obtain 1.65 and 1.69 for the lower and upper bounds, respectively, with a significance level α of 0.05. If we choose a significance level of 0.01 instead, the results are 1.52 and 1.56 for the lower and upper bounds, respectively. A rule of thumb suggests that test statistic values in the range of 1.5 to 2.5 are relatively normal. In any case the results obtained with this statistical test are in general agreement with those obtained with the autocorrelation function for one time lag the degree of precision being a matter of how rigorous the research needs to be.

We make use again of statistical software to compute the test statistic and plot the results averaged over the period of study as filled contours. Contour lines enclose the area delimited by the upper bound of critical values.

3.2.8 Residuals as a function of the wind

Our interest in analysing whether the residuals are somehow correlated with the magnitude of the wind speed arises from Thorndike and Colony's proposal (section 2.2.1) that the free drift solution exhibits two different, limiting behaviours depending on the intensity of the wind; that in fact two different regimes exist: one for weak winds with a non-linear response of the ice, and another for strong winds with a linear response of the ice. Because it is not easy to deduce, a priori, a wind magnitude that marks the transition between the two regimes, its value being highly dependent on the ice structure or rheology, we look instead for any indication of change correlated with the magnitude of wind speed. We suspect that the linear model fails at very low wind speeds. And it is therefore by comparing the residuals against the wind speed that we hope to detect such a change, if there is any.

In order to investigate this further we proceed by plotting the absolute values of the residuals, $|e|$, against the absolute value of the wind speed, $|U_a|$, and we do that in two ways. Firstly, we normalize the absolute values of the residuals by the corresponding absolute value of the ice drift speed, $|u|$, and plot the resulting ratio, $|e|/|u|$, against the absolute value of the wind speed. Then we normalize also the absolute value of the wind speed by the corresponding absolute value of the ice drift speed, $|U_a|/|u|$, and plot $|e|/|u|$ vs. $|U_a|/|u|$. We do that for selected grid points at different locations along the Arctic basin for the winters from 1978-79 till 2003-04. For the sample being representative we select points both off the coast and in the center of the basin. We use graphical means to check for correlation between residuals and winds because the latter, the independent variable in this context, is a continuous magnitude and that complicates the use of standard statistical test. Usually, the independent variable in correlation tests is time, which is easily approximated as discrete by the use of time lags. The impracticability of performing a graphical analysis of all grid points restricts us to do so on a few grid points.

Chapter 4

Results

"Pack-ice might be described as a gigantic and interminable jigsaw-puzzle devised by nature."

Ernest Shackleton, "South!"

4.1 Mean fields

As a stepping stone from where to start building the explanation of the results we firstly present mean fields for the data variables on which we base our analysis (sea ice drift, wind) and then we do the same for the solution parameters of the inverse problem ($|A|$, θ and C). The data shown are averages over winter seasons (October through May) and over the years 1978-79 to 2003-04.

The time-mean ice drift $\vec{u}$ and wind U_a fields are shown in figure 4.1. The main AGC features are clearly recognizable on both plots which, in addition, match quite accurately one another. That resemblance is not by coincidence as the ice drift mean field pattern reflects roughly equal contributions by winds and surface currents [Thorndike and Colony, 1982], the latter to a large degree ultimately wind-driven and moving in general in the same sense as the ice motion [Coachman and Aargaard, 1974; Thorndike and Colony, 1982].

We don't find significant differences in the general pattern of the AGC between our mean field and the one from [Kimura and Wakatsuchi, 2000], despite theirs covering a much shorter period of study (winters from 1991-92 to 1997-98) than ours, which gives us confidence in the reliability on our dataset.

4.1.1 Inverse problem solution: A and C

$|A|$ and θ

Next we present the mean fields of both components of the A parameter, namely its magnitude and its angle, for the period of study (figure 4.2).

The magnitude of the A parameter reaches its lowest values off the coast of the Canadian Archipelago and Greenland, an area known to be covered by the thickest MYI, and gradually increases towards the Central Arctic and areas covered with seasonal sea ice. Low values are also found by the coast in the East Siberian Sea. The ice in this region is fundamentally FYI so thickness is not an issue here, but certainly coastal geometry is. Maximum values are reached in the Barents Sea and Baffin Bay. The significant spatial variability we find for this parameter is most likely associated with changes in internal ice stress, a sea

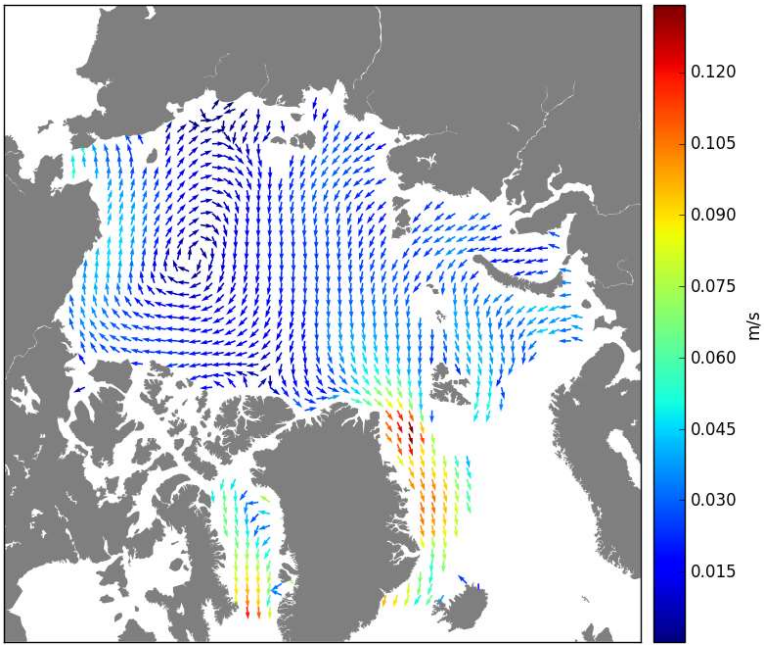

(A) Sea ice drift

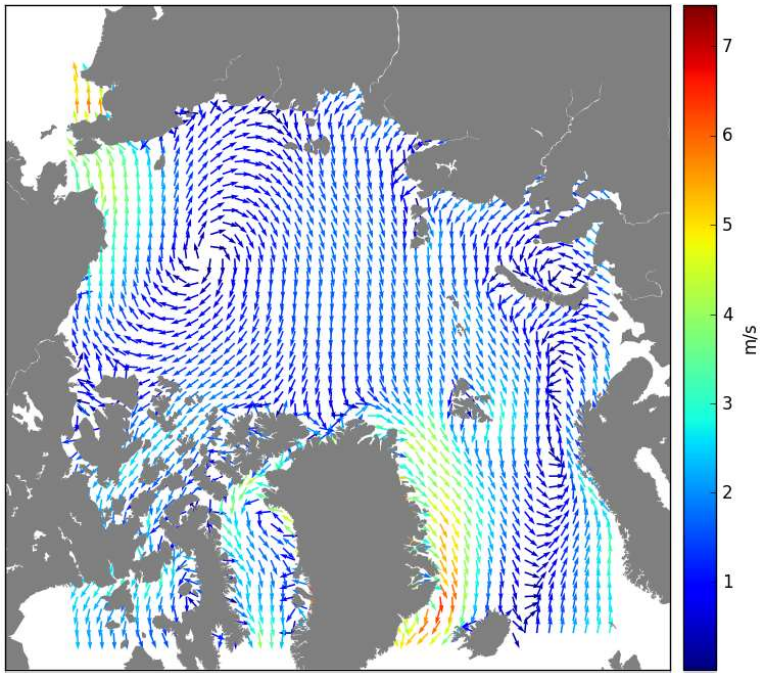

(B) Winds (10 m.)

FIGURE 4.1: Mean velocity fields for the period $1978/79 - 2003/04$

ice characteristic that is strongly dependant on ice strength and consequently its thickness. [Thorndike and Colony, 1982] didn't find any evidence of geographical variation for the $|A|$ parameter but, as indicated by [Kwok et al., 2013], their data was probably biased because it was obtained from buoys preferentially deployed in multi-year ice that, at that time (1979-1980), was much thicker than today's [Kwok and Rothrock, 2009].

The A parameter also includes directional information. The turning angle shows almost exclusively negative values, indicating clockwise rotation , as expected in the Northern Hemisphere. The very few positive angle values that show up in spots of Barents and Greenland seas are most probably the result of measurement noise. The mean field for the turning angle, θ, shows progressively decreasing values towards the south from a maximum in the central Arctic, reaching minimum values just off the coasts almost everywhere around the basin, probably due to coastal effects, and also at the ice edge. As for $|A|$, the turning angle in the region close to the Arctic Archipelago shows minimum values.

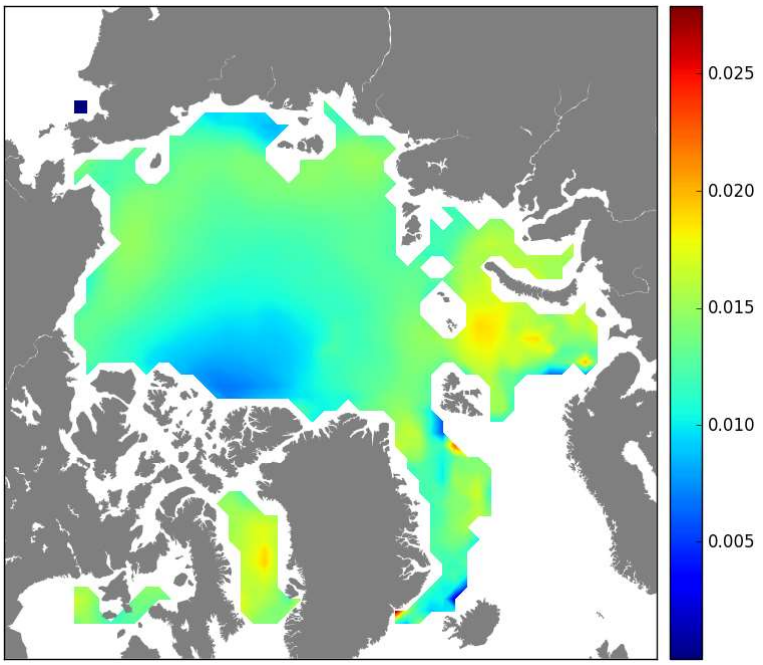

(A) $|A|$

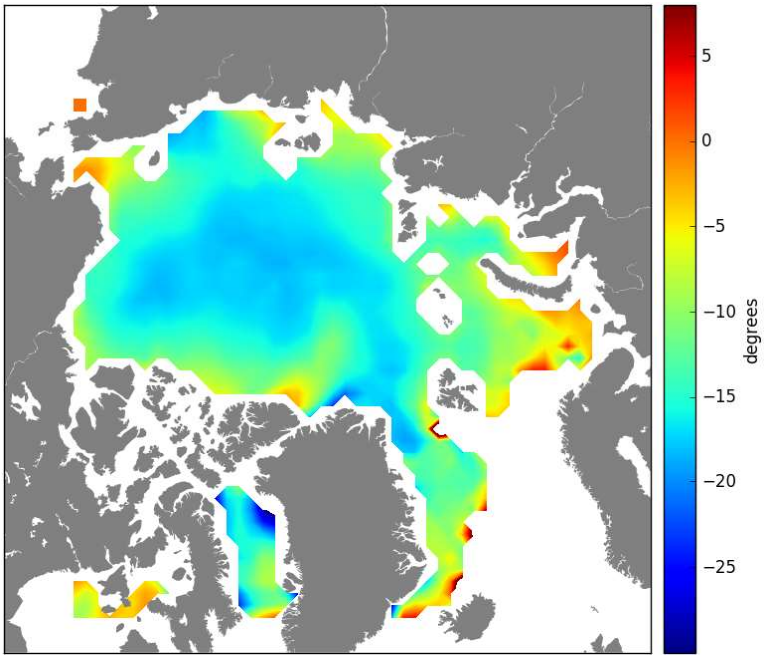

(B) θ

FIGURE 4.2: Mean fields for the period 1978/79 - 2003/04

U_w: Geostrophic ocean surface currents

The intercept of the linear model, $\vec{U_w}$, represents the time-mean geostrophic ocean currents (Figure 4.3), that is, the portion of the ice motion that is constant over a given interval of time and hence not linearly related to the local wind. The component of the current that is linearly related to the wind, if indeed such a component exists, is incorporated in the first term of the linear equation 2.10 [Kwok et al., 2013].

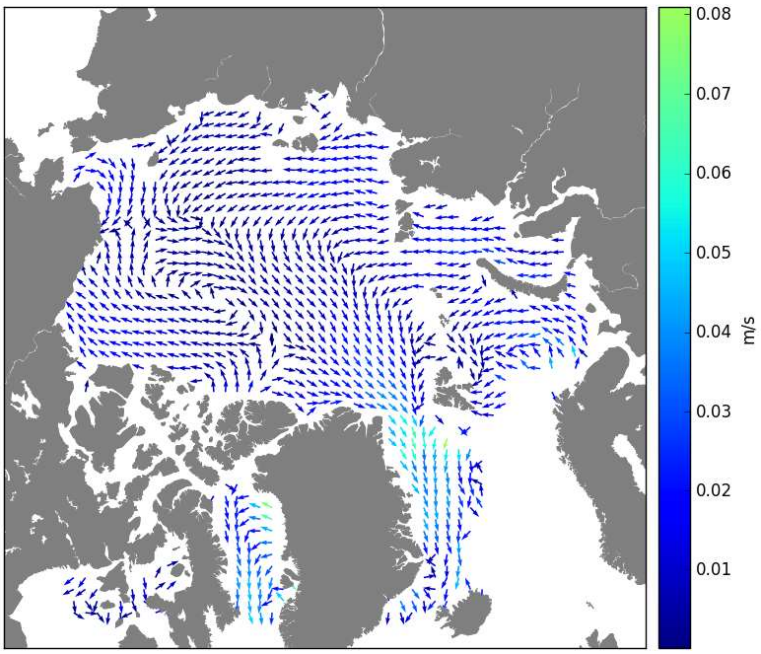

FIGURE 4.3: Sea currents main field for the period 1978/79 - 2003/04

[Thorndike and Colony, 1982] admonished that if one is to interpret $\vec{U_w}$ as the time-mean sea currents the linear model has to be proven reliable. We will assess the goodness of fit of the model in the section 4.2. For now, we compare our modelled sea currents velocity field against a geostrophic currents velocity field derived from dynamic topography (data details in section 3.1.3). The comparison is done over a shorter period (1993-2002) than the one employed for the rest of mean fields in this section (figure 4.4). Our solution for the new period of reference matches the main features of the Arctic circulation (Beaufort Gyre, Transpolar drift, Pacific inflow, East Greenland Current) as reproduced by the geostrophic field quite accurately. The differences between the two velocity fields arise most probably from short-term variability, which in the case of our model will be registered by the error estimate or residuals.

4.2 How good is the model?

4.2.1 R^2: coefficient of determination

For the majority of the Arctic Ocean, the fractional variance of the ice drift explained by the model, i.e. attributed to the wind stress ranges within 65-75% (figure 4.5). Along the coasts of the Arctic basin, and in Baffin Bay and the Greenland Sea it reduces to 50% or even less. Clearly other forces are counteracting the effects of the wind stress in these areas.

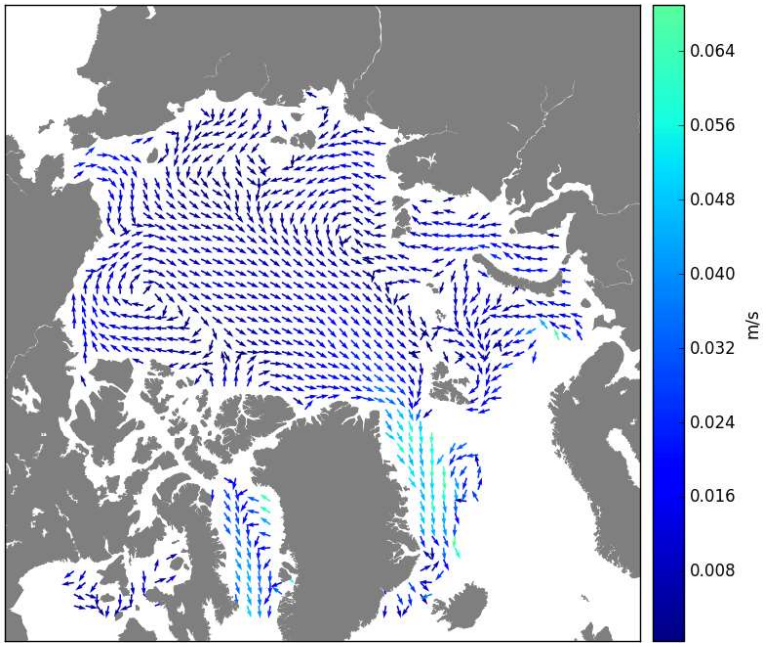

(A) Inverse method

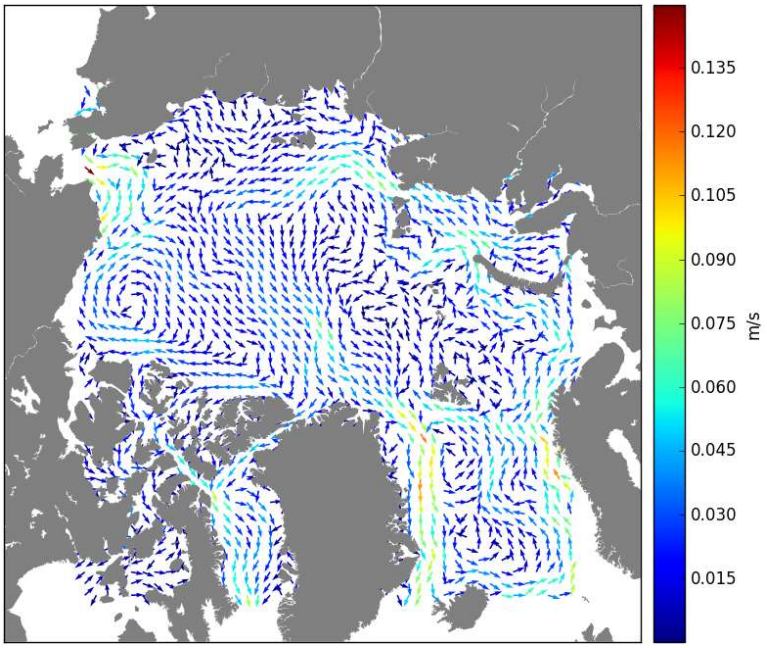

(B) Sea Surface Height from FOAM

FIGURE 4.4: Sea surface currents mean fields for the period 1993-2002

Lower values of R^2 imply more activity of the physical effects grouped together in the error estimates or residuals: some physical effects operate near the coasts to weaken the linear relationship (correlation) between the ice velocity and the wind. Likely candidates are mechanical constraints on the ice drift in the form of coastal geometry, the effects of internal ice stresses and time varying ocean currents.

The areas off the coast in the Arctic basin show a consistent pattern of values around 0.55-0.65. Here internal ice stresses are certainly playing a role due to the proximity of the

coast. North of the Canadian Archipelago the thicker ice surely reinforces the coastal effect on the ice internal stress even further and lowers R^2 values to 0.50. The lowest values for R^2 within the Arctic basin are registered in the coastal regions of East Siberian Sea and also in Barents Sea, again as a consequence of some counteracting forcing not related to ice thickness because the area is covered by FYI. Geometry of the coast is most probably the cause in the former. The lowest values of them all are those registered along the eastern Greenland coast and in Baffin Bay, most probably due to the presence of strong and variables currents in those areas [Thorndike and Colony, 1982].

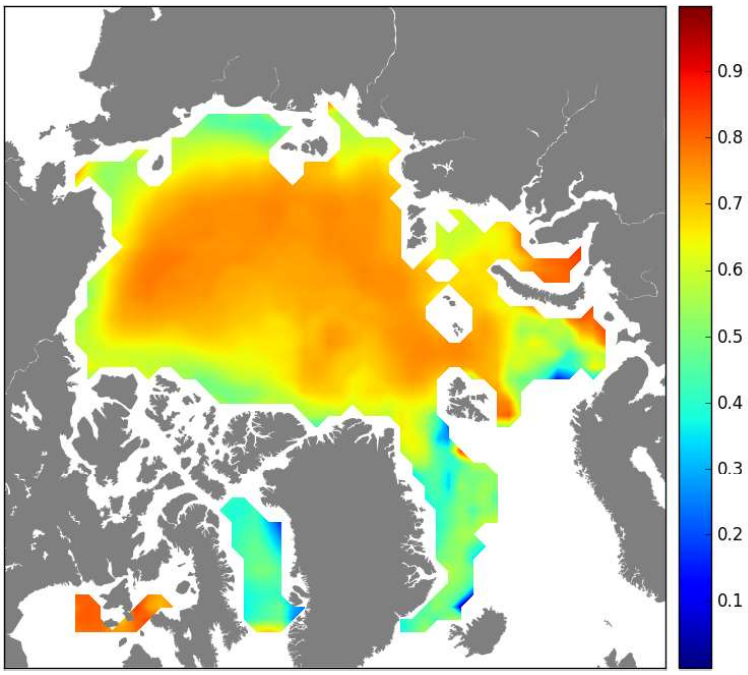

FIGURE 4.5: R^2 mean field for the period 1978/79 - 2003/04

4.2.2 Residuals

Figure 4.6 shows the RMS of the residuals by components. Over most of the Arctic basin the values of both components of the residuals are systematically higher near the coast than in the central Arctic. This is particularly true in the Kara, Laptev, East Siberian and Chukchi seas, specially for the x component, and also along the coast of Alaska, though this last area doesn't show any particular difference between components. We presume that this proximity to the coast is the main cause behind this behaviour, because it enhances the effects of the internal stresses in the ice, which in turn tend to reduce the correlation between wind and sea ice motion [Kwok et al, 2013] [[and reflects a worse performance of the linear model]].

However, that general coastal pattern changes off the Canadian Archipelago. The values of the x component in this region, despite being slightly lower than in the other areas discussed above, are still higher than in the central Arctic. But that is not the case for the y component, which shows values similar to those of the central Arctic instead. This behaviour hints at different dynamics along the x axis, that seem to be more constrained in that direction than in the other. This is somehow paradoxical and unexpected, specially if we take into account that this is the region with the thickest ice concentration and that the

regression that originated the residuals was performed on winter data, when the conditions are theoretically less favourable for the model.

In eastern Greenland the values of both components are higher than in the center of the basin, especially those of the y component which increases markedly further south. This makes quite a lot of sense since this region is known to be under the influence of strong sea currents. The flow being predominantly southward, it is not a surprise that the component that reflects a bigger residual [[and hence, a bigger lack of fit of the model]] is the one that accounts for the north-south direction.

The other two regions with high residual values are Barents Sea and Baffin Bay. The latter, as it was the case for eastern Greenland, is dominated by strong and variable sea currents, which is reflected in both residual components but specially on the y component. The former, despite being an area almost 100% covered by FYI that is not particularly constrained by coastal geometry, reflects some of the highest values for both components. The only reason we can think about for this results is the presence of variable currents in the area. But we don't have ways to confirm this guess.

Are residuals normally distributed?

Figures 4.7 and 4.8 show the results of the statistical analyses to assess the normality of the residuals. In spite of their having been obtained with two different statistical tests, namely Anderson-Darling (AD) and Shapiro-Wilk (SW), each one based on a completely different theoretical approach, the results are remarkably similar. We also note that they have been performed only on residuals obtained from winter data, when the conditions are theoretically less favourable for the validity of the model.

Both components of the residuals comply with the normality assumption, and they do that for both tests, in big areas of the central Arctic (those within black contours), where internal ice stress is lower than along the coasts even in winter. The contours include areas with a ratio statistic/critical values lower that one (dark blue) for the AD test, and statistic values higher than 0.97 (dark orange) for the SW test (section 3.2.6). Even the central areas outside those contours deviate only slightly from normality for both tests. Where the ice stress is expected to be high, due to thicker ice as in northern Canada or due to coastal geometry as in East Siberian Sea, the normality assumption fails. The same can be said of eastern Greenland, this time the cause being most probably the strong sea currents that dominate in that area. The main differences between both tests arise in Barents and Greenland seas, where the residuals are mostly normal in some of those areas according to AD but not for SW.

Are residuals uncorrelated?

With regard to the second assumption for randomness of the residuals (figures 4.9 and 4.10 again both tests, Autocorrelation function (AC) and Durbin-Watson (DW), show similar results by components which, as before, we interpret as a sign of reliability.

However, and in clear contrast with the normality tests results, where x and y components roughly matched each other on both tests, there's barely any agreement between

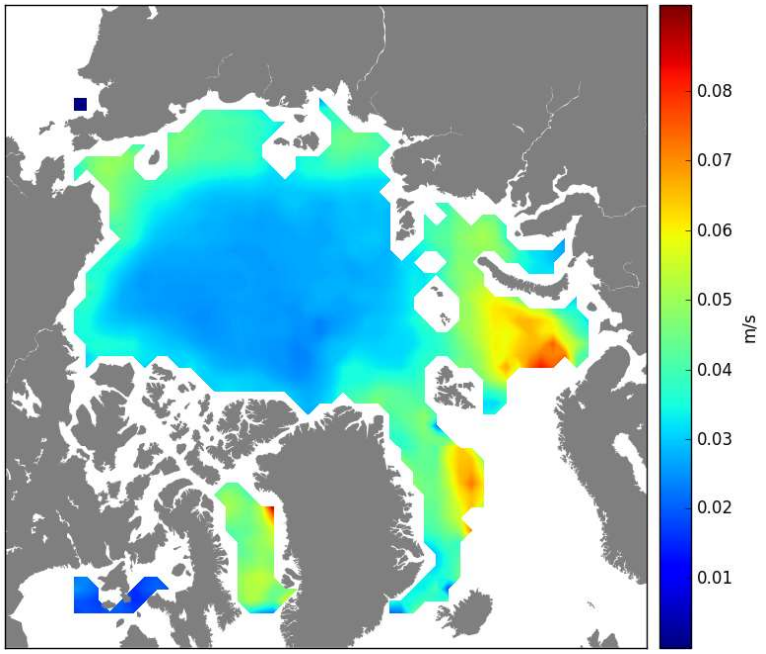

(A) Real (u)

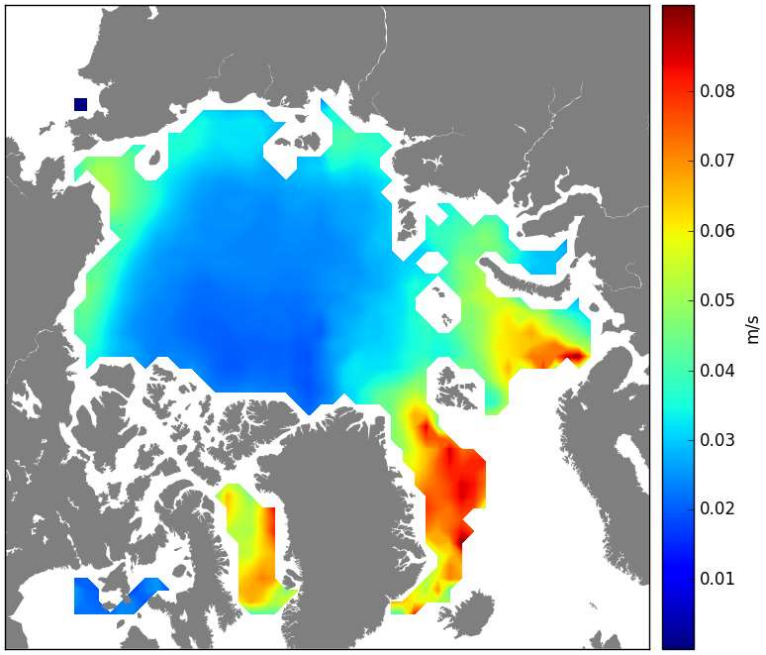

(B) Imaginary (v)

FIGURE 4.6: u and v components of the residuals for the period 1978-2004

components in the correlation tests results. The x component of both AC and DW statistics shows high correlation values (areas within the black contours) off Canada and in East Siberian and Chukchi seas, extending way off the coast into the central Arctic. The contours include areas with values above 0.2 (dark orange/red) for the Autocorrelation function, and statistic values higher than the critical value upper bound of 1.56 (dark blue) for the SW test (section 3.2.6). On the other hand, the y component exhibits high values off Alaska, also extending into the center of the basin, and in small areas off Ellesmere Island and north and east of Greenland.

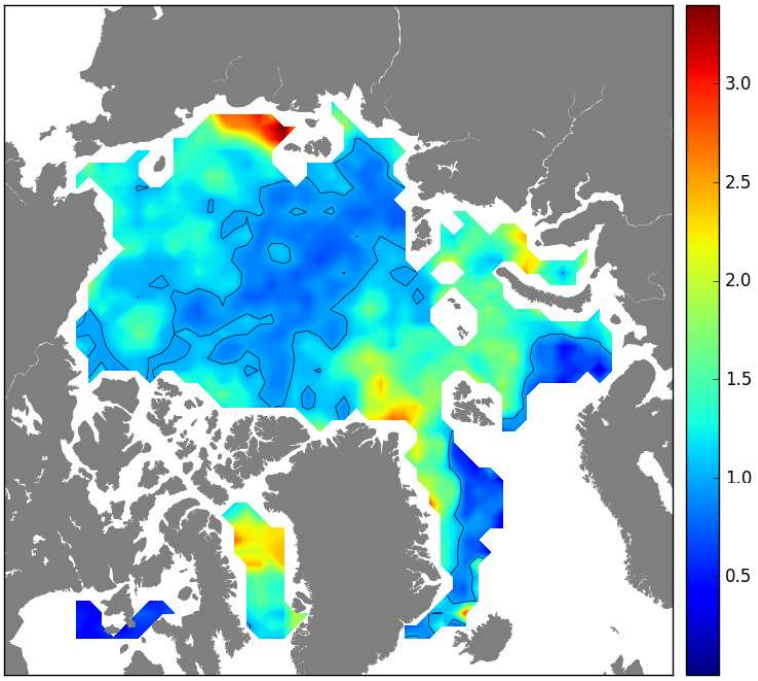

(A) Real

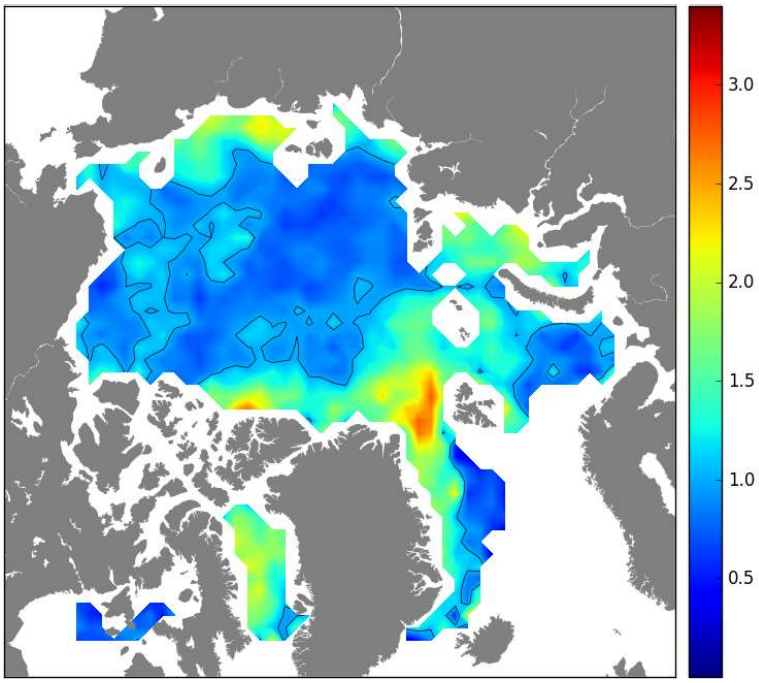

(B) Imaginary

FIGURE 4.7: Anderson-Darling statistical test for the period 1978-2004

Coastal and ice thickness effects seem to be behind correlation in all these areas, but the mismatch detected between the results of both components hints at another factor, maybe less relevant when checking for normality and that shows up now. The fact that component results show such a different behaviour makes us think that maybe the wind is involved, at least more than it could have been when assessing normality.

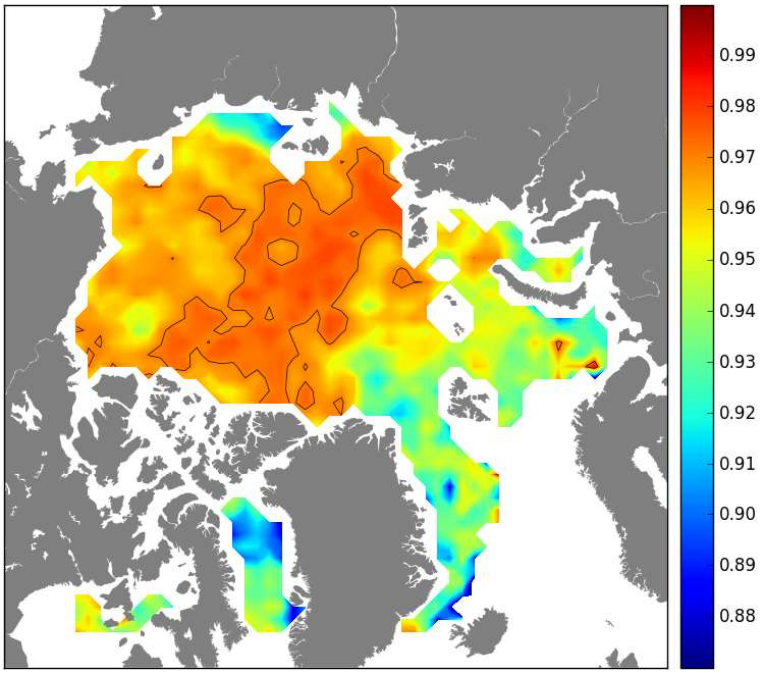

(A) Real

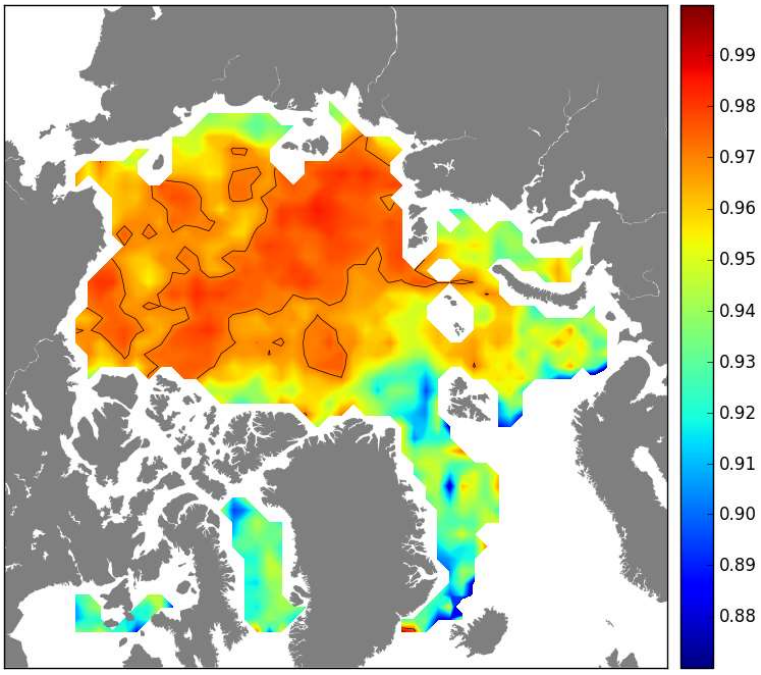

(B) Imaginary

FIGURE 4.8: Shapiro-Wilk statistical test for the period 1978-2004

Are residuals independents of winds?

As a result of comparing the normalized residuals against the magnitude of the wind $|U_a|$ (top of figures 4.12 and 4.13) we detect a slightly decreasing trend of the ratio $|e|/|u|$ for low wind speeds and then the trend flattens out at higher wind speeds. That pattern is general throughout the Arctic, though the slope varies between locations. There seems to be a resemblance with the shift of drift regime from a non-linear to a linear one mentioned

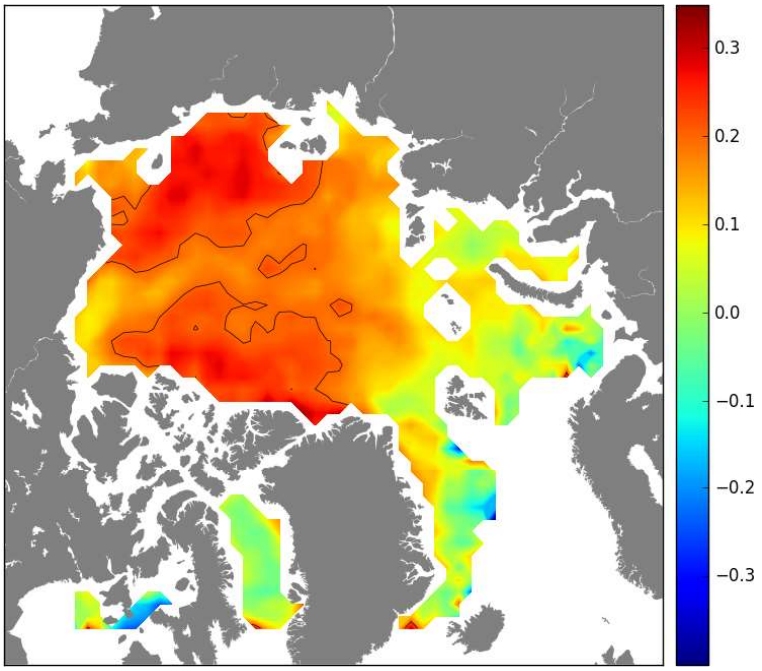

(A) Real

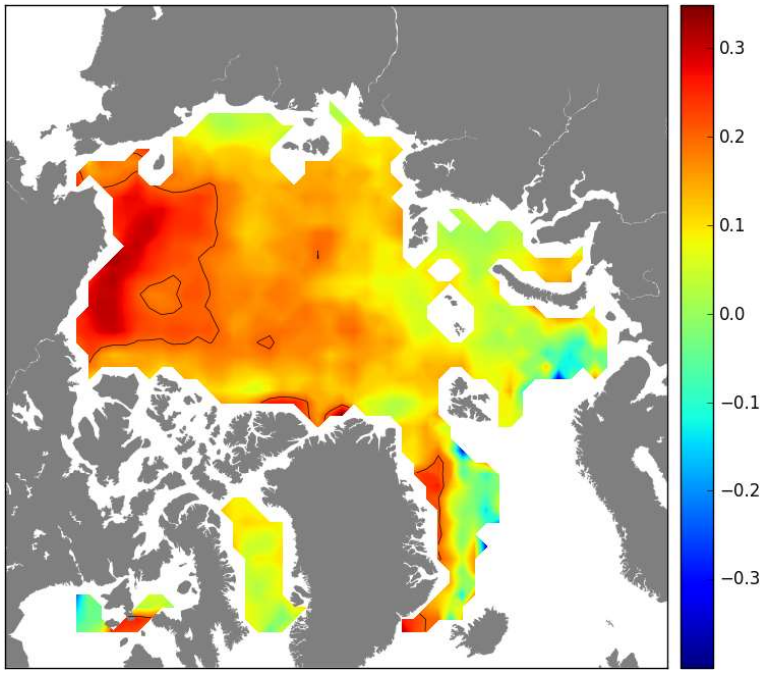

(B) Imaginary

FIGURE 4.9: Autocorrelation function average results for the period 1978/79 – 2003/04

by [Thorndike and Colony, 1982] as the wind speed increases. The regional variability in slope values hints at different behaviour of the model depending on both wind regimes and sea ice conditions but we have no means of verifying this guess. On the other hand, these results inform also of a certain negative correlation between residuals and low values of wind speed. That correlation seems to weaken as the wind speed increases.

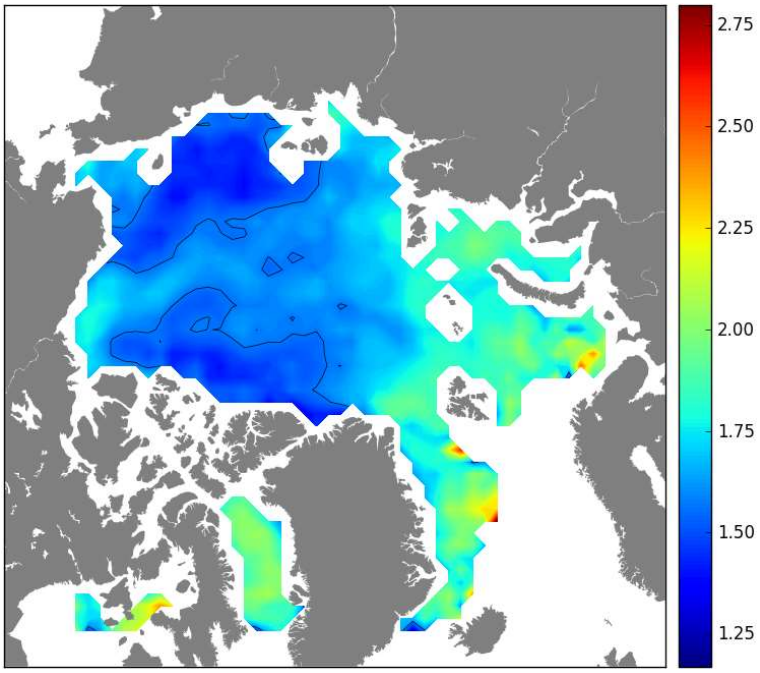

(A) Real

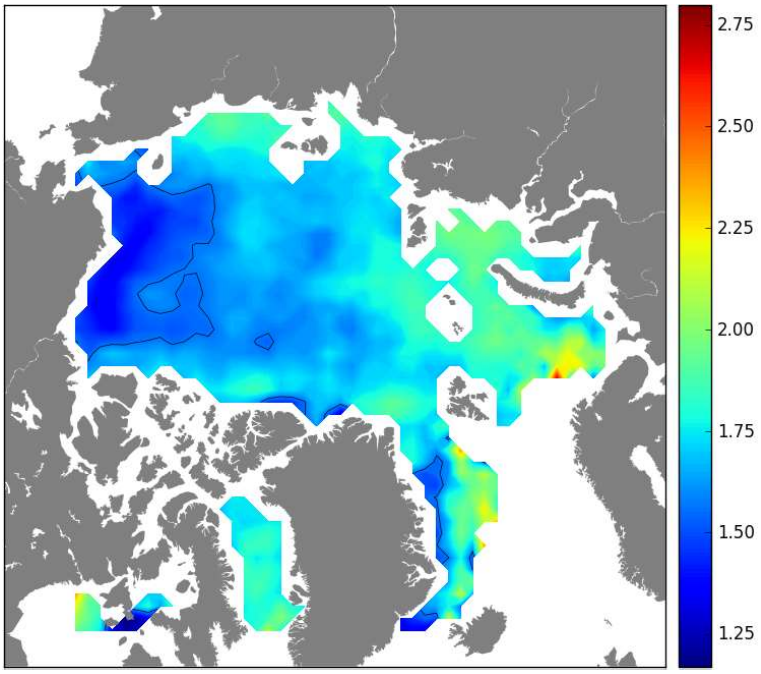

(B) Imaginary

FIGURE 4.10: Durbin-Watson statistic average values for the period 1978/79 – 2003/04

When the comparison is done between both normalized variables, $|e|/|u|$ and $|U_a|/|u|$, a much different and clearer pattern emerges (bottom of figures 4.12 and 4.13). The ratio $|e|/|u|$ decreases rapidly from around 1 to 0.01 as the normalized wind ratio $|U_a|/|u|$ increases from 10 to 100. From that point onwards, the normalized residuals and wind ratios increase in unison. The breaking point is then located at $|U_a|/|u|$ equalling around 100. At that point the

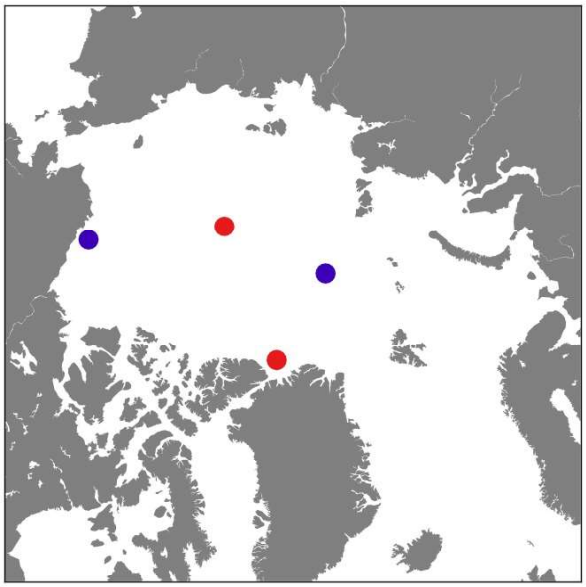

FIGURE 4.11: Distribution of points of our grid

normalized residuals are the smallest and we hence infer that this normalized wind value represents the ratio at which the model achieves its best performance. That means a wind speed around two orders of magnitude stronger than the ice drift speed. Any deviation from that ratio value highlights the presence of other forcings, in addition to the wind and the ocean currents stresses, acting on the ice and causing the model to perform worse.

At higher $|U_a|/|u|$ values we interpret that despite the wind blowing harder and harder there is very little response from the ice, most probably due to the effect of its own internal stresses or the obstructing effect of geographical features. When the ratio $|U_a|/|u|$ falls below 100 the wind speed becomes less than two orders of magnitude higher than the ice drift speed. In this regime we suspect that sea currents come into play and hamper somehow the effect of the wind.

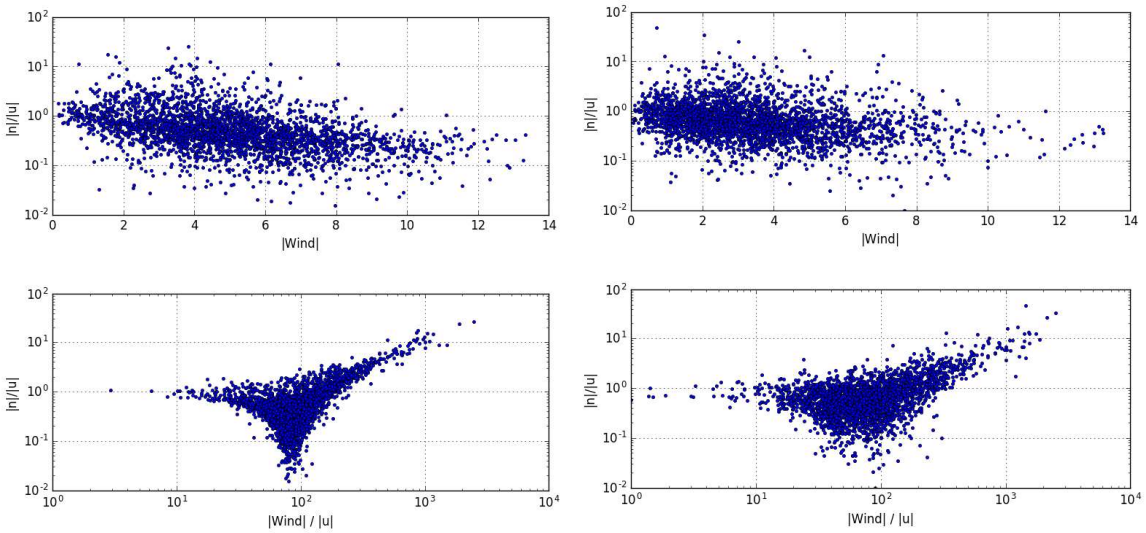

(A) Central Arctic (B) Off Greenland's coast

FIGURE 4.12: $|Res|/|u|$ vs. $|wind|$ at red locations for the period 1978-2004

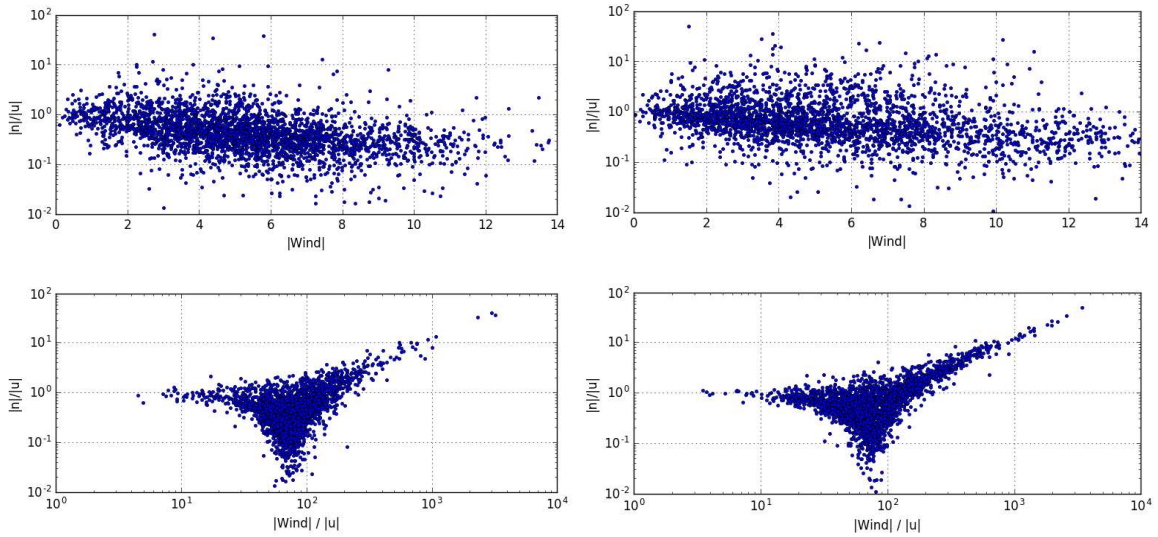

(A) Central Arctic (B) Off Alaskas's coast

FIGURE 4.13: $|Res|/|u|$ vs. $|wind|/|u|$ at blue locations for the period 1978-2004

4.3 Seasonal variability

We base our analysis of the seasonal variability on the dataset from MET Norway which covers the whole year for the period from October 2012 to September 2015. We define winter as the period from October till May, both months included, and summer as the period from June till September.

4.3.1 $|A|$ and θ

Changes in $|A|$ and θ in time and space tell us about changes in the coupling between wind and ice, and about changes in the internal ice stresses that tend to hamper ice motion [Kwok et al., 2013]. According to the same authors this seasonal variability can be explained by two different effects.

The first one is due to a seasonal change in the structure of the atmospheric boundary layer that manifests itself by changes in the relationship between the geostrophic wind (G) and the wind at 10 m. (U_a) from winter to summer. [Thorndike and Colony, 1982] refer to an analysis by [Albright, 1980] where the ratio U_a/G increased from 0.55 to 0.60 and the clockwise angle between U_a and G decreased from 30° to 24°, between summer and winter. From those results they infer that for the same geostrophic wind the stress on the ice should increase by 10-20%, due to the fact that the wind stress varies as the square of the wind velocity (equation 2.7), and 6° further to the right in summer than in winter. If the ice velocity responds in a uniform way to the surface stress, the magnitude of A would be larger in summer by this 10-20% and θ larger by 6°. However, they also report that the observed seasonal changes in $|A|$ and θ are about twice as large, so this effect on its own cannot account for the whole seasonal variability. Although they don't specifically mention it, we assume that the above argumentation can be extended from the 10 m. wind all the way down to the surface. But because we are using 10 m. winds instead of geostrophic winds as they do in their analysis, we infer that this effect is almost negligible in our case

(the distance between an altitude of 10 m. and the top of the boundary layer being much bigger than 10 m.)

The second effect relates to changes in the internal ice stresses. Due to melting, ice looses strength during the summer, which in turn relaxes its internal stress. The opposite happens in winter. The net effect of the ice stress must be to dissipate energy, and therefore to resist wind stress [Thorndike and Colony, 1982]. Hence, this mechanism predicts that $|A|$ and θ would be smaller in winter, when greater stresses are expected, than in the summer, when the ice pack is nearly free of internal stresses.

When analysing the magnitudes of the A parameter (figure 4.14) we observe that its value increases in summer throughout the entire basin, except for Chukchi Sea, where it actually decreases. We recall the fact that the dataset on which this analysis is based covers only three seasons, maybe not long enough a time series to cancel out all short-term variability. We are inclined to attribute this deviation from the general trend to this effect.

The angle θ experiences an even clearer seasonal change than $|A|$ (figure 4.15). All regions in the Arctic basin but a tiny spot in the East Siberian Sea register a notable increase in the values of θ again most probably due to the weakening of sea ice as a consequence of summer melting. There are much less internal ice stresses and the ice can drift almost freely with the wind.

4.3.2 U_w: Geostrophic ocean surface currents

Figure 4.16) shows that the pattern of sea currents doesn't seem to change appreciably with the seasons, the only remarkable differences being a slight intensification of the Beaufort Gyre north of Alaska and the Canadian Archipelago, and also of the Transpolar Drift in the Central Arctic plus a more meandering pattern of the latter during summer.

4.3.3 R^2: coefficient of determination

We report regional and seasonal variability for this parameter as per figure 4.17). Away from the coast the values for the summer are consistently larger than those for the winter. The lowest values are found near the coasts both during summer and winter.

Although with the present data set we cannot discriminate between the effects responsible for the coastal pattern, there are indications that the ice stress is the cause. The strongest evidence is the proximity of the coast. R^2 rises north of Alaska in the summer, when the ice pack loses contact with the coast. The data suggests that the ice stress gradients play a larger role near the coasts and a smaller role away from them.

Low ice-wind correlations are also found along the eastern coast of Greenland. This is a region of high average and highly variable currents [Thorndike and Colony, 1982] which probably accounts for the low correlation. Low values show up as well near the coasts of the East Siberian Sea, probably induced by the coastal geometry rather than ice thickness.

4.3.4 Residuals

Figure 4.18 presents a somehow contradictory seasonal distribution of the residuals. Theoretically, the ice conditions would be more favourable for the linear model in study during the summer than during the winter. The summer heating induces melting of the ice cover,

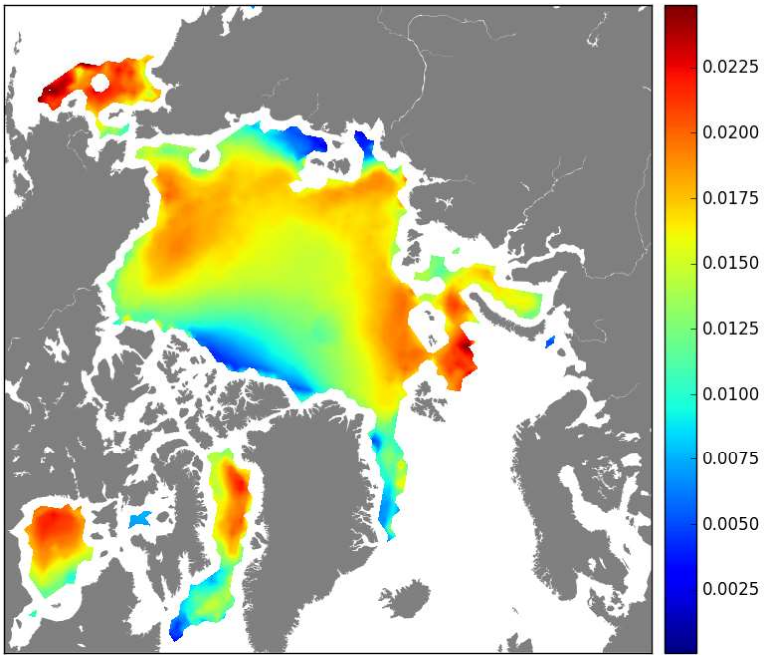

(A) Winter

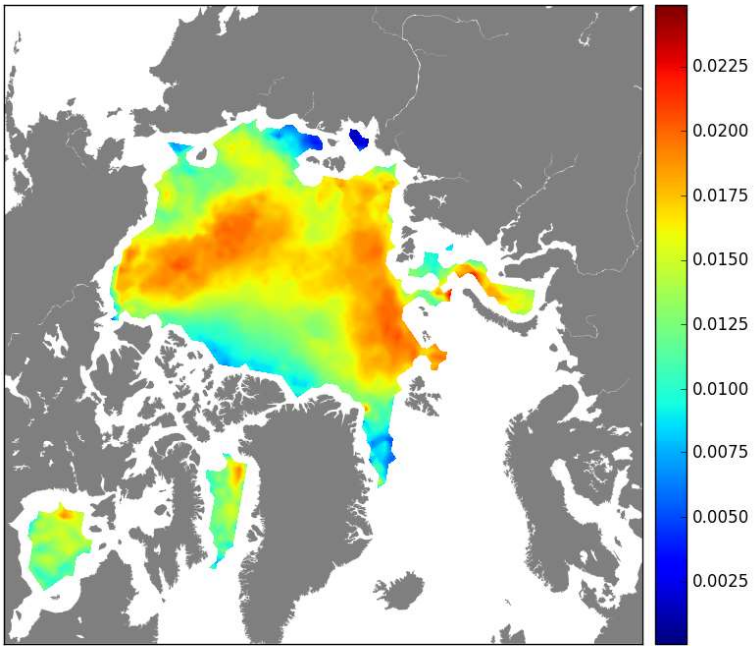

(B) Summer

FIGURE 4.14: $|A|$ seasonal evolution for the period 2012 - 2015

which in turn reduces the strength of the sea ice and its internal stresses. As a consequence of this seasonal changes sea ice can drift more freely. According to this, the residuals are expected to be smaller in summer than in winter, but in fact they are much larger in general during the summer and the situation affect both components of the residual.

We must recall at this point that MET Norway, the provider of the same dataset on which this seasonal analysis is based, has problems with the remote sensing data for sea ice drift during the summer. They suffer from a noisy signal during that season due to a denser

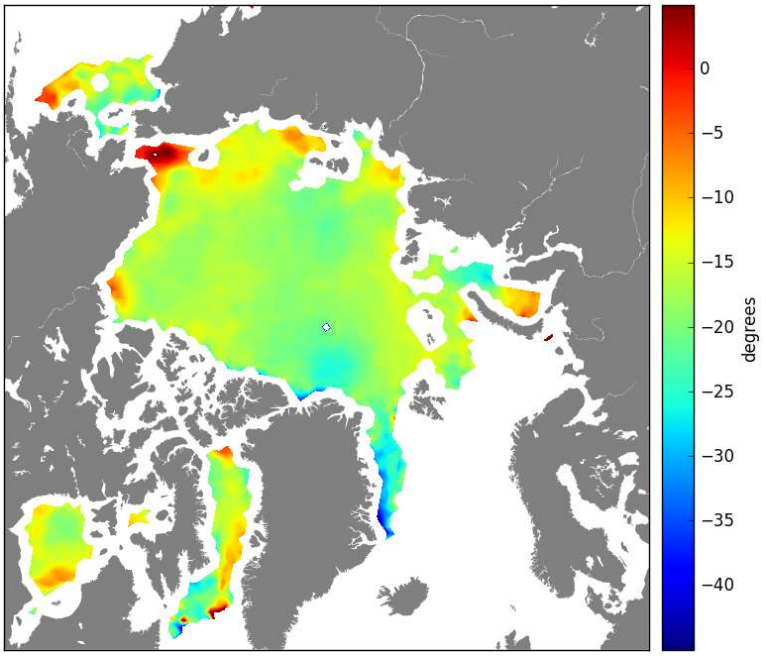

(A) Winter

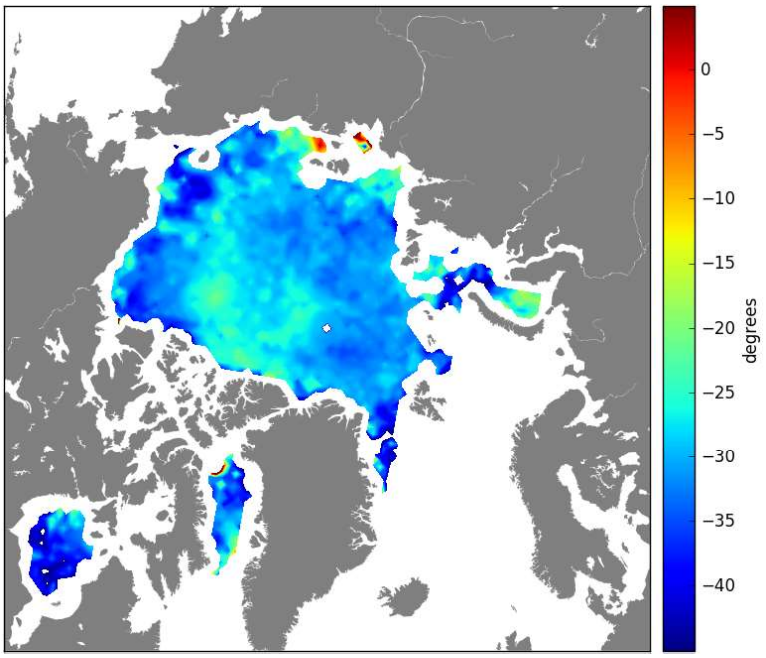

(B) Summer

FIGURE 4.15: θ seasonal evolution for the period 2012 - 2015

atmosphere. Because it is precisely at that time of the year that we get doubtful results, we are seriously tempted to think that both circumstances are related. If that is the case we then have to face the question of how reliable are the all other results obtained from this same dataset. In principle, all the results obtained for the other parameters are within reasonable dimensions and comply with all a priori assumptions made in regard to sea ice characteristics and also with the literature [Thorndike and Colony, 1982; Kwok et al., 2013]. Therefore, we will consider that summer anomaly on the residuals simply as noise.

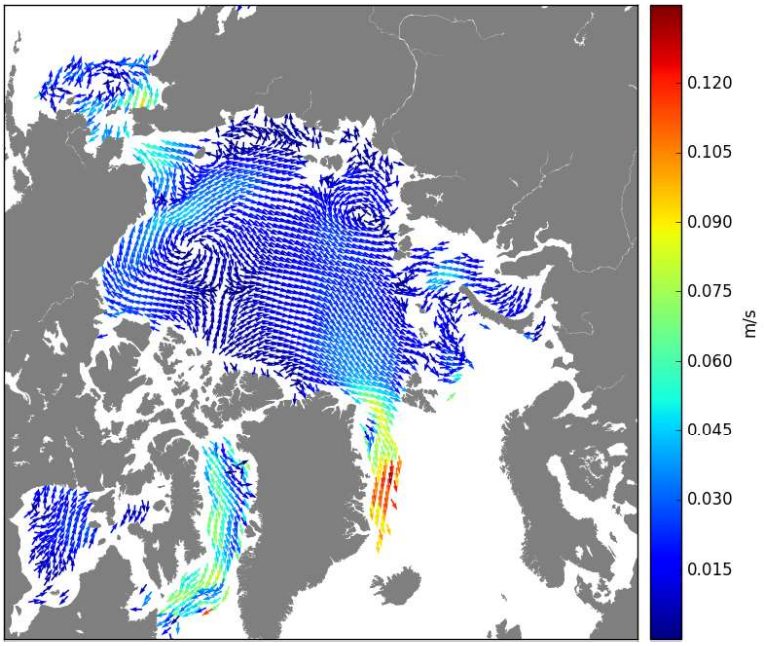

(A) Winter

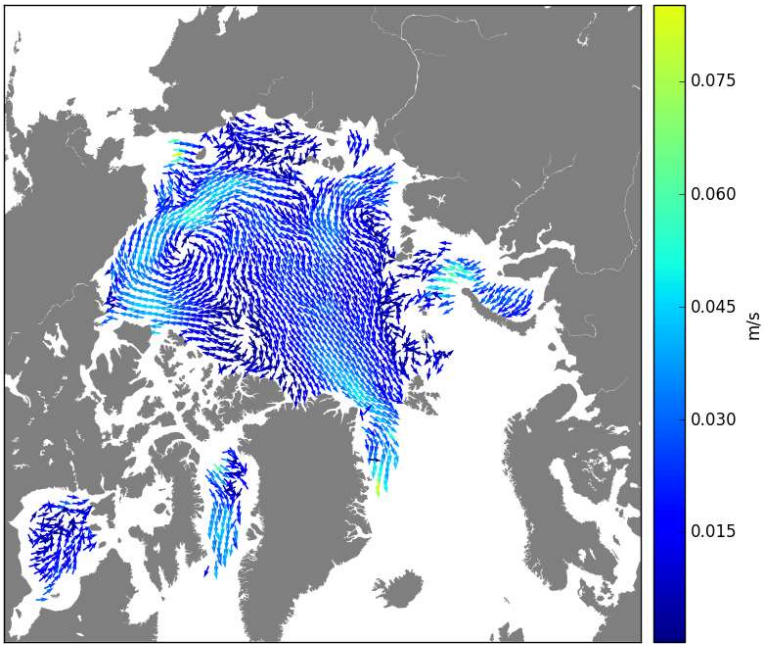

(B) Summer

FIGURE 4.16: Sea Currents seasonal evolution

4.4 Decadal variability

To analyse the long-term evolution of the performance of the model we perform a linear regression for the sea ice parameters resulting from solving the inverse problem, namely $|A|$, θ and U_w plus R^2 and the residuals, on their respective yearly averages to determine the sign of their trends for the period of reference.

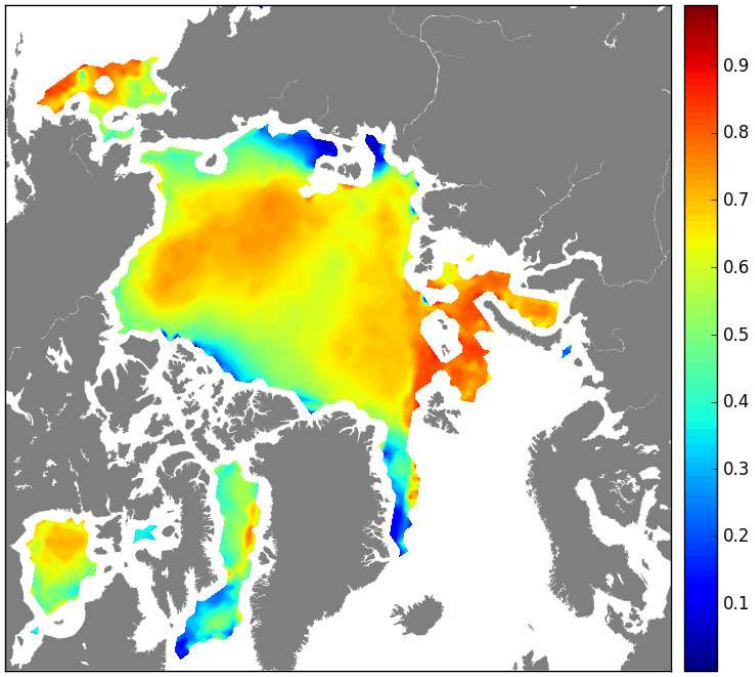

(A) Winter

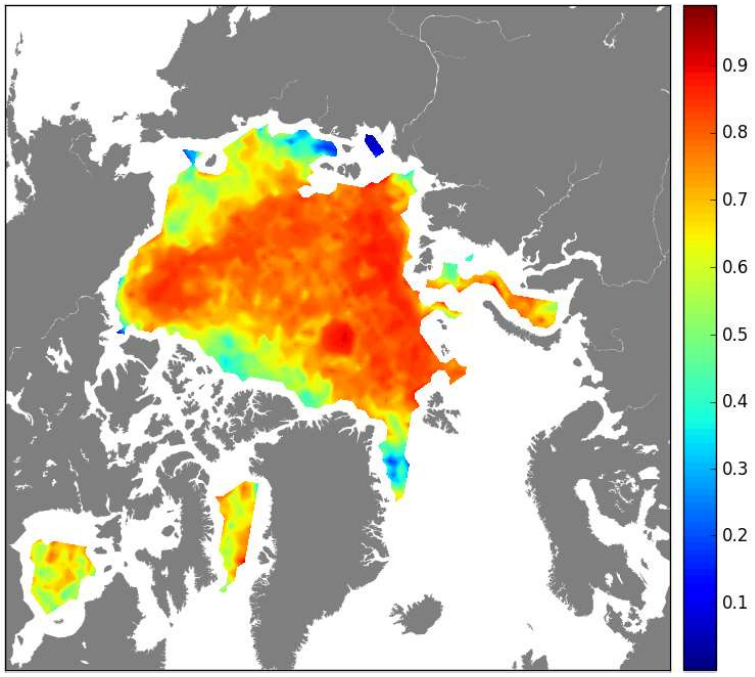

(B) Summer

FIGURE 4.17: R^2 seasonal evolution

4.4.1 $|A|$ and θ

The values of the $|A|$ parameter have experienced a net increase throughout the entire Arctic region in the 26 years period analysed here. This increase is clearly confirmed by the regression performed on the yearly averages for the entire period of study. All the Arctic except Baffin Bay, a well defined area north of Greenland, another between the island of Novaya Zemlia and mainland Russia in the Kara Sea and much smaller spots in the Laptev,

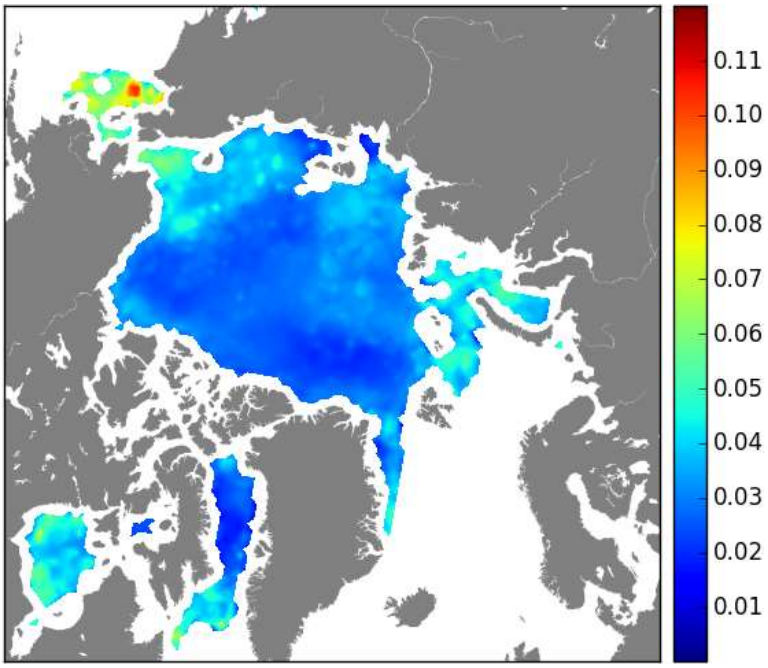

(A) Winter

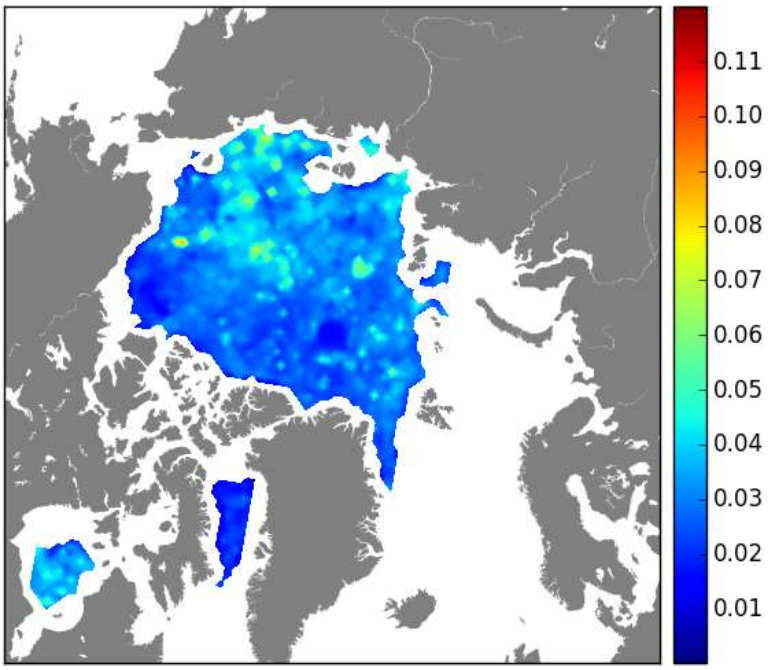

(B) Summer

FIGURE 4.18: Seasonal evolution of real component of residuals (2012-13 2014-15)

Greenland and Barents seas show a clearly positive slope in the multi-decadal trend. This seems to be an unambiguous sign of a change in the structure of sea ice, most probably its thickness.

With respect to the θ parameter it is important to note that, because of the standard angle notation already discussed in the section 2.2.1 (clockwise angles are negative), the signs of the slopes for the decadal evolution of the θ parameter are inverted with respect to those of the other parameters discussed. A negative slope actually represents an increase in the

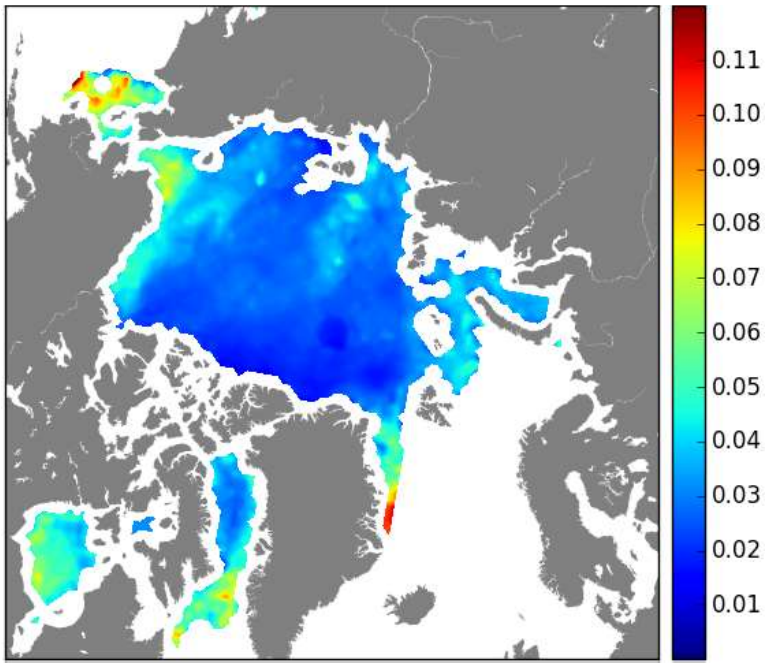

(A) Winter

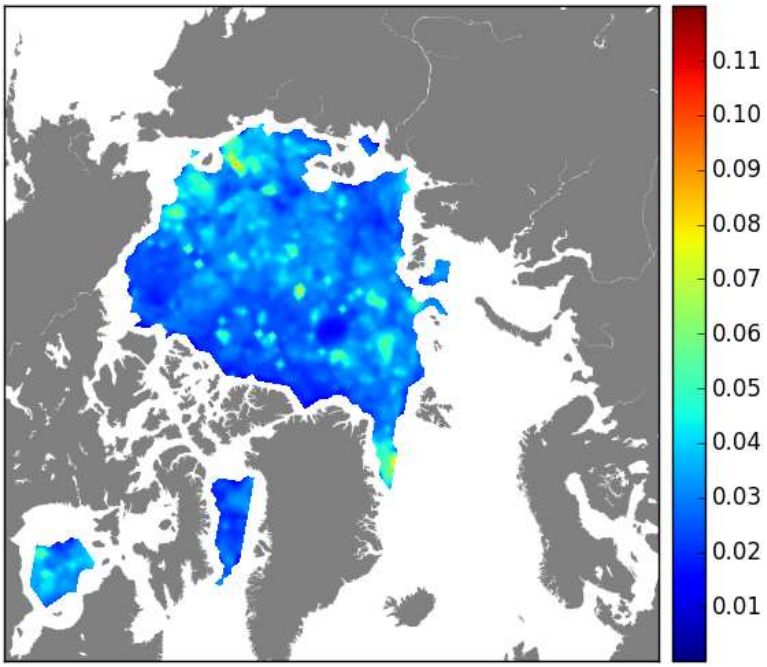

(B) Summer

FIGURE 4.19: Seasonal evolution of imaginary component of residuals (2012-13 2014-15)

clockwise angles and vice versa. We have dismissed the option of computing the regression on the absolute value of the angles due to the fact that, despite being very few, there are locations where positive angles exist and then positive and negative angles will be mixed together.

The θ parameter doesn't show such a clear trend as $|A|$ (figure 4.21). There seems to be a net decrease of the angle between the wind and the ice drift for most of the central

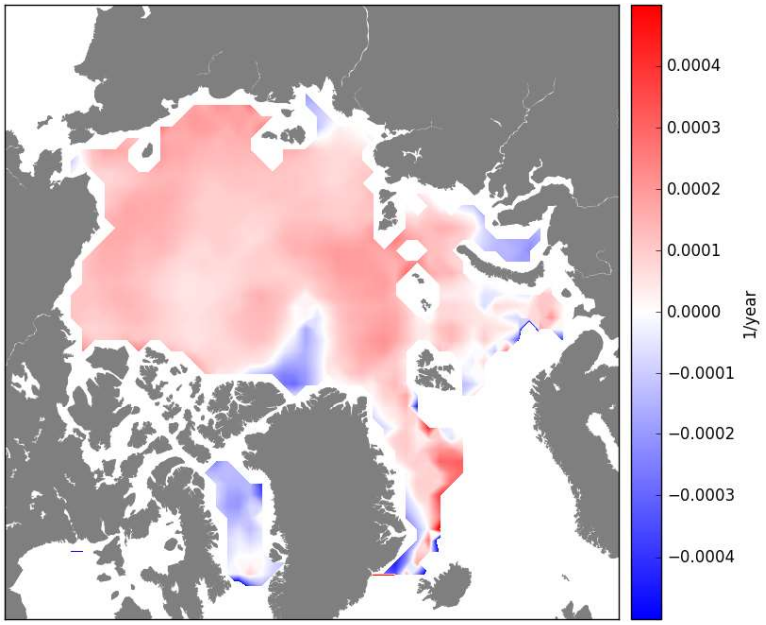

FIGURE 4.20: Least squares of $|A|$ for the period 1978/79 - 2003/04

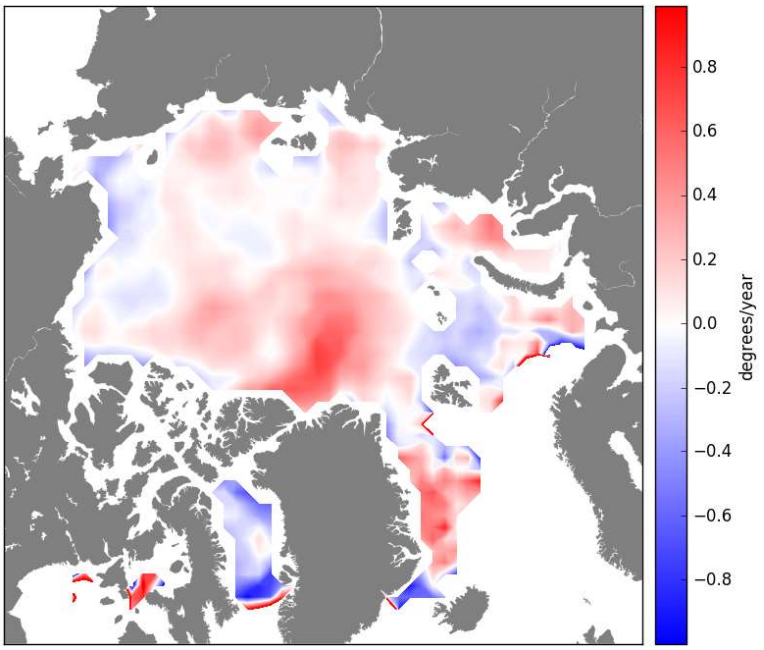

FIGURE 4.21: Least squares of $|\theta|$ for the period 1978/79 - 2003/04

Arctic, notably in the regions that extend between northern Greenland and the North Pole, and north of the Canadian Archipelago. The values also go down in the Greenland Sea. The situation changes in the marginal sea ice zones, with a less marked decrease in the East Siberian, Kara and Laptev seas, and an increase, though not too strong, in the Chukchi, Beaufort and Barents seas, and definitely a strong rise of the values of this parameter in Baffin Bay.

As $|A|$ and θ intertwine to constitute the complex A parameter, the behaviour of both parameter components must be somehow related. But the generalized rise in magnitude observed for $|A|$ is not completely mimicked by θ; clearly some other forcing is coming

into play here, the most plausible candidate being the ocean currents, which are in fact the second element responsible for the drift of sea ice in the proposed linear model. We hypothesize that the effect of the magnitude of the currents on the mostly wind-induced sea ice drift is much less significant than the effect of the direction of that underwater flow This would explain both the homogeneous increasing trend observed in the values of $|A|$ and the more heterogeneous trend in the values of θ.

4.4.2 U_w: Geostrophic ocean surface currents

The sea currents in this linear model are assumed to be in steady state for seasonal time scales and shorter but, as any other geophysical variable, they undergo changes in the long term. The regression performed for the whole period shows a rising sea currents speed trend in the center of the basin, in the western side of Baffin Bay and in the Greenland Sea, and a speed reduction trend for the rest of the Arctic. But the numbers obtained are very small, barely undistinguishable from zero, and most probably statistically insignificant.

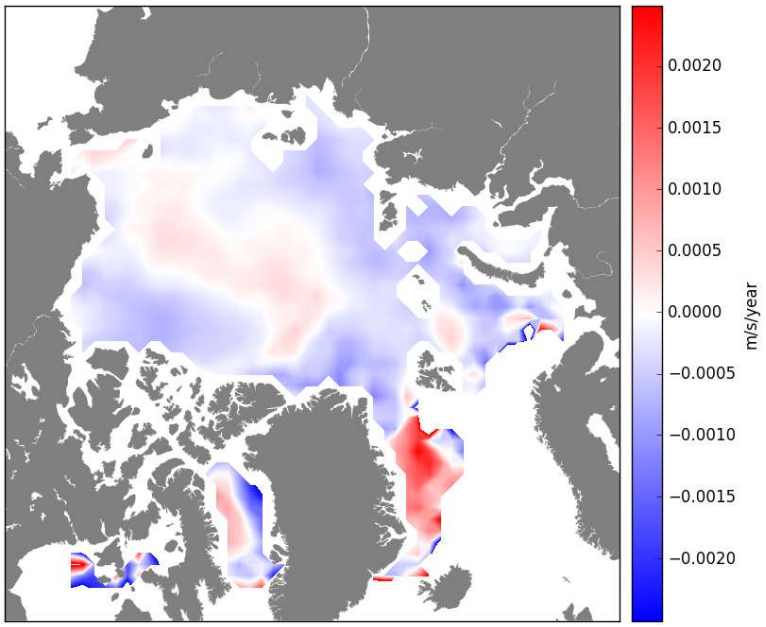

FIGURE 4.22: Least squares of $|C|$ for the period 1978/79 - 2003/04

4.4.3 R^2: coefficient of determination

The trend for the coefficient of determination, R^2 (figure 4.23), shows that the whole Arctic basin has shifted to a regime where nearly all areas have reached levels for the variance attributed to the wind stress as high as 70% and sometimes above that.

The rise in the values of the R^2 parameter are even more generalized than those of $|A|$, with only the region north of Greenland and two small coastal areas, in the Kara and Greenland seas, showing a negative trend. The linear regression over the entire period shows that the bigger increments have taken place in coastal areas, whether they are covered with FYI or even with MYI.

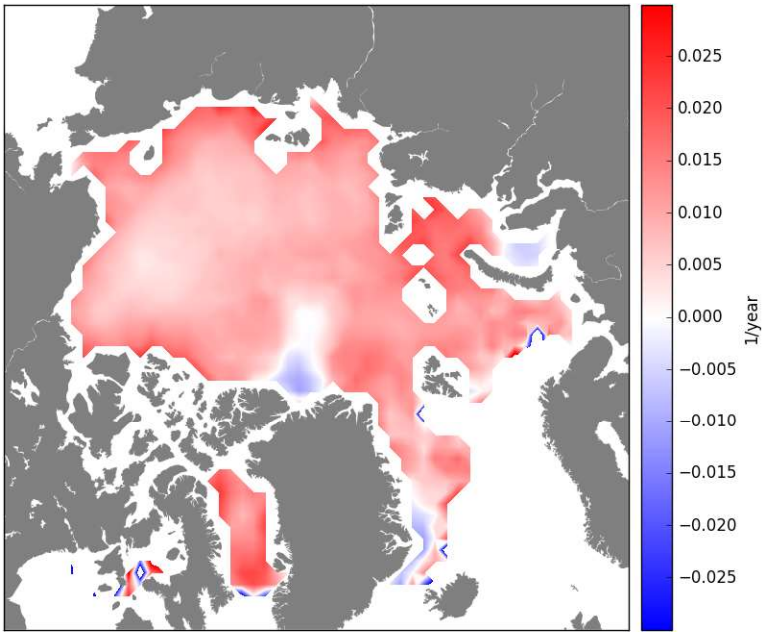

FIGURE 4.23: Least squares of $|R2|$ for the period 1978/79 - 2003/04

4.4.4 Residuals

In full agreement with the results analysed so far for the other parameters, both components of the residuals show a clear decrease for the period of reference (figures 4.24 and 4.25) In principle, a decrease in the magnitude of the RMS of the residuals can be interpreted as an improvement of the model, based on the interpretation of the RMS as the its standard deviation. The smaller the RMS of the residuals, the smaller the standard deviation of the observed data around the modelled values.

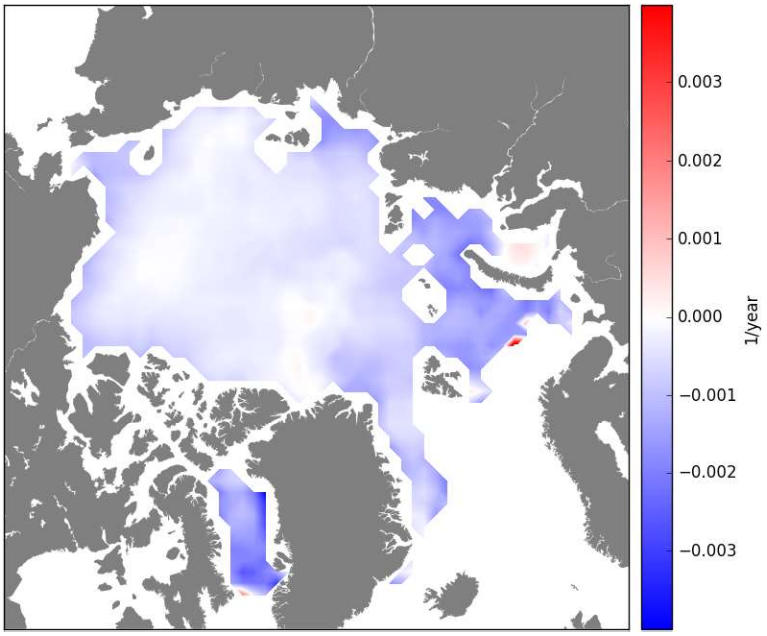

FIGURE 4.24: Least squares of $|A|$ for the period 1978/79 - 2003/04

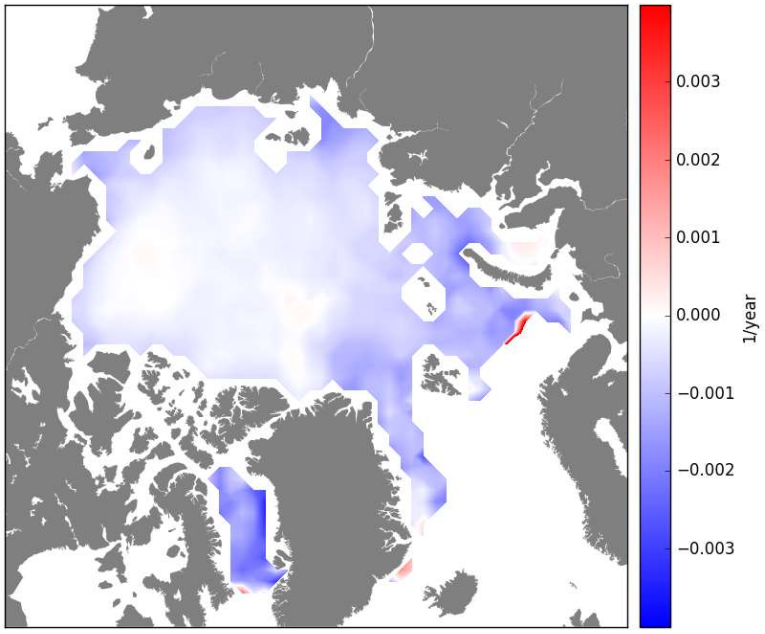

FIGURE 4.25: Least squares of $|A|$ for the period 1978/79 - 2003/04

It has to be noted, however, that the quality of the data along the whole period (1978-2004) is not homogeneous. From 1987 onwards more satellite observations were incorporated, resulting in an improved dataset. At least part of the reported long-term increases can be attributed to this circumstance. Nonetheless, we have confirmed through other graphical analysis that the increasing trend has continued after that date, hinting at the fact that the increment is real and not an artifact from the data.

Chapter 5

Conclusions

"May you live in interesting times!"

Ancient chinese curse

In this thesis we have solved and also assessed the validity of a linear model of sea ice drift of the form $\vec{u} = A\vec{U}_a + \vec{U}_{wg}$, where $A = |A|e^{i\theta}$. This model represents one solution for the free drift regime, which is a simplification of the equation of momentum of sea ice that neglects internal sea ice stresses.

We have employed an inverse method technique, in essence a linear regression on observational surface wind and sea ice drift data, to solve for the model parameters $|A|$, θ and U_{wg}, and computed the residuals resulting from the least squares regression as an estimate of the model's performance. This information can be then used to solve for the lineal model in a "forward" sense and make independent estimates of sea ice drift to complement estimates of MET Norway based on remote sensing. The coefficient of determination, R^2, has also been computed to provide us with complementary information about the relationship between wind and sea ice drift.

The validity of the model has been assessed through the analysis of the residuals. We have checked with standard statistical tests whether they take on a Gaussian structure and are free of temporal correlations to confirm they are random noise. Failing to prove so basically means that those residuals contain information about the process not accurately captured by the model and, hence, its applicability is in question. That information could refer to e.g. neglected sea ice stress (in relation to ice thickness or the effect of coasts) or sea currents variability. Besides, we have also analysed the possible correlation between the residuals and the wind.

We have follow three earlier studies [Thorndike and Colony, 1982; Kimura and Wakatsuchi, 2000; Kwok et al., 2013], with the significant difference that they have all employed geostrophic wind measurements while we have used 10 m. surface winds instead. Also, the time periods analysed differ in length and seasons covered. But despite this heterogeneity some comparisons have been made.

A general assessment of the model has been performed for the period 1978-2004, as a result of which time-mean fields for $|A|$, θ, U_{wg}, R^2 and the residuals have been produced. Regional differences detected on $|A|$, θ and R^2 have been explained in terms of a priori assumptions about sea ice internal stresses, ice thickness, the effect of coastal geometry and variable geostrophic sea currents.

At a first glance, the regional distribution of $|A|$ seems to be correlated with sea ice thickness while, in contrast, θ seems to be correlated with distance from the coast. A closer look reveals more details. Besides thickness, $|A|$ values are also affected to a lesser degree by coastal effects. In the case of θ, the influence of sea ice thickness shows up clearly north of Canada superimposed on the effect of the coast. The other model parameter, U_{wg}, has been positively assessed against geostrophic currents derived from modelled Sea Surface Heights. Overall, those time-mean fields are largely in agreement with those studies mentioned above.

The coefficient of determination R^2 suggests that the model performs better away from the coasts and on thinner sea ice. With respect to the residuals, these results would point to a higher susceptibility to coastal effects than to ice thickness effects, both in relation to internal sea ice stress. We find this circumstance somehow paradoxical and believe that it motivates for further research.

In order to accept the above results as fully reliable we need to prove the randomly nature of the residuals as much as possible. The results from statistical tests reproduced in this thesis have been performed on the winter dataset, theoretically the time of the year less favourable for the performance of the model due to bigger sea ice stresses.

Large regions of the Arctic basin show residuals that comply with normality and have small autocorrelation. However, this circumstance is not applicable to all regions, specially those close to the coast or that have a thicker sea ice cover. Residuals also show non-random behaviour in marginal areas like Greenland and Barents seas, and Baffin Bay. Besides, it has been detected that they correlate with very low wind speeds. In that regime the relationship between sea ice drift and wind shifts from linear to non-linear [Thorndike and Colony, 1982] and, hence, the model fails.

A detailed statistical analysis for the summer would have been desirable to complement the above information. But the full season dataset amounts to only three years and therefore statistical robustness is poor. Being that short, we presume that annual variability has not been smooth down and that the results are not fully reliable. For these reasons we do not present plots of statistical tests from that dataset. However, we report that the results for the summer are better than those for the winter, for both normality and autocorrelation tests, as in fact should be expected due to the very different ice conditions between seasons.

Seasonal differences are clearly confirmed for both components of the A parameter, $|A|$ and θ, and also for the coefficient of determination. We cannot say the same about the ocean currents, which do not seem to vary appreciably in between seasons.

If we focus in particular on the A parameter, we can make comparisons with results from the literature. It has been reported that both parameters are generally larger during the summer than during the winter [Thorndike and Colony, 1982; Kwok et al., 2013]. In particular, [Thorndike and Colony, 1982] obtain an average winter estimate of 0.077 for $|A|$ and -5 degrees for θ, and an average summer estimate of 0.011 and -18 degrees, respectively. [Kwok et al., 2013] obtain an average winter estimate of 0.009 ± 0.0015 for $|A|$ and -1.9 ± 2.6 degrees for θ, and an average summer estimate of 0.01 ± 0.001 and -7.1 ± 3.6 degrees, respectively. We also obtain larger values for both $|A|$ and θ during the summer than during the winter, though our values are slightly larger than the ones from the studies mentioned above. We report a summer average estimate of 0.014 ± 0.003 for A and -32.09 ± 6.85 degrees for θ, and a winter average estimate of 0.014 ± 0.004 and -17.03 ± 7.95, respectively.

The difference in magnitude between our values and those obtained in the other two studies could be a direct consequence of the recent acceleration of the thinning of the Arctic ice cover reported by several authors [Rothrock et al., 2008; Kwok and Rothrock, 2009]. Despite being short, our full-year dataset covers a more recent period (2012-2015) than those employed in the studies of [Kwok et al., 2013] (1982-2009) and specially [Thorndike and Colony, 1982] (1979-1980).

The results of least squares regressions performed on annual means of the winter dataset show an unequivocal long-term increase from the late 1970s in the values of $|A|$ for almost the entire Arctic basin. An even more clearly positive trend is detected from the regression on R^2 values, clearly indicating an increase of the variance of the sea ice drift attributed to the wind stress over time. On the other hand, the slope of the regression on both components of the residuals are negatives over most of the Arctic. Only marginal spots that could be easily identified as noise show positive trends. The prospects for the linear model under consideration seem to be improving over time.

According to some authors there is a confirmed increased trend in sea ice drift speed that cannot be explained by a corresponding increase in wind speed. The most plausible explanation argued for this drift acceleration is a thinning of the sea ice cover [Spreen et al., 2011]. This single fact is enough to explain the positive trend for $|A|$ in relatively easy and straightforward terms.

The $|A|$ parameter depends on the densities and drag coefficients on the ice surface of both the air above and the water underneath (2.12). As the densities can be considered constants, the reason for the change in the value of the parameter through time has necessarily to be related with a change in any, or both, of the drag coefficients. Those coefficients vary with the roughness of the surface.

Due to the way it is formed, MYI is always rougher than FYI. Because the surface and bottom roughness are so well correlated, it would be expected that the air-ice and the water-ice drag coefficients for a certain ice cover would be correlated as well. But the difference in roughness should be relatively much greater for water drag than for air drag because the oceanic boundary layer (OBL) under ice is only about 30 meters thick while the atmospheric boundary layer (ABL) is some 1000 meters thick. Thus an ice ridge with, for example, a height of about 1 meter above the surface and hence an underwater keel depth of about 5 meters would protrude through only a negligible fraction of the ABL, having a tiny effect on the air-ice drag coefficient, C_a. Its keel, however, protrudes through a significant fraction of the OBL and has a bigger effect on the water-ice drag coefficient, C_w. We expect, therefore, form drag to be a more important component of C_w than of C_a.

It can then be inferred that a change to a new sea ice regime with more younger and less older ice will result in an increase of the $|A|$ parameter as the one reported here. If form drag has a bigger effect on the the water-ice drag coefficient than in the air-ice one, a thinning of the Arctic sea ice cover will cause the former to decrease more than the latter and, assuming the densities to be constant, that will cause $|A|$ to increase. This argument seems to be valid for $|A|$ but there remains the question of what causes such a big value for θ.

The combined results obtained in this thesis point to the possibility of the model being moderately reliable to make estimates of sea ice drift in certain regions of the Arctic basin during the winter, mainly away from the coast. Our confidence increases notably for the

summer, with probably most of the basin suitable for its application. The only possible exceptions would be the region closest to the Canadian Archipelago, due to its thick ice, and East Siberian Sea, because of its coastal geometry. The prospects are not so good in marginal Arctic areas like Eastern Greenland and Baffin Bay, due to the permanent presence of strong and variable sea currents.

Appendix A

Least squares solution for the linear inverse problem

$$E = e^T e = (d - Gm)^T (d - Gm) = \sum_{i=1}^{N} \Big[d_i - \sum_{j=1}^{M} G_{ij} m_j \Big] \Big[d_i - \sum_{k=1}^{M} G_{ik} m_k \Big] \tag{A.1}$$

The indices on the sums within the parentheses are different dummy variables, to prevent confusion.

Multiplying out the terms and reversing the order of the summations lead to

$$E = \sum_{j=1}^{M} \sum_{k=1}^{M} m_j m_k \sum_{i=1}^{N} G_{ij} G_{ik} - 2 \sum_{j=1}^{N} m_j \sum_{i=1}^{N} G_{ij} d_i + \sum_{i=1}^{N} d_i d_i \tag{A.2}$$

We now compute the derivatives $\frac{\partial E}{\partial m_q}$ term by term.

For the first one it gives

$$\frac{\partial}{\partial m_q} \Big[\sum_{j=1}^{M} \sum_{k=1}^{M} m_j m_k \sum_{i=1}^{N} G_{ij} G_{ik} \Big] = \sum_{j=1}^{M} \sum_{k=1}^{M} [\delta_{jq} m_k + m_j \delta_{kq}] \sum_{i=1}^{N} G_{ij} G_{ik} = 2 \sum_{k=1}^{M} m_k \sum_{i=1}^{N} G_{iq} G_{ik} \tag{A.3}$$

Since the model parameters are independent variables, derivatives of the form $\frac{\partial m_i}{\partial m_j}$ are either unity, when $i = j$, or zero, when $i \neq j$. Thus, $\frac{\partial m_i}{\partial m_j}$ is just the Kronecker delta δ_{ij} and the formula containing it can be simplified trivially.

The second term gives

$$\frac{\partial}{\partial m_q} \Big[-2 \sum_{j=1}^{N} m_j \sum_{i=1}^{N} G_{ij} d_i \Big] = -2 \sum_{j=1}^{N} \delta_{jq} \sum_{i=1}^{N} G_{ij} d_i = -2 \sum_{i=1}^{N} G_{iq} d_i \tag{A.4}$$

The third term does not contain any model parameters, so

$$\frac{\partial}{\partial m_q} \Big[\sum_{i=1}^{N} d_i d_i \Big] = 0 \tag{A.5}$$

Combining the three terms it gives

$$\frac{\partial E}{\partial m_q} = 2 \sum_{k=1}^{M} m_k \sum_{i=1}^{N} G_{iq} G_{ik} + -2 \sum_{i=1}^{N} G_{iq} d_i = 0 \tag{A.6}$$

Writing this equation in matrix notation yields

$$G^T Gm - G^T d^{obs} = 0 \tag{A.7}$$

If $[G^T G]^{-}1$ exists we arrive at the following estimate of the model parameters:

$$m^{est} = [G^T G]^{-1} G^T d^{obs} \tag{A.8}$$

which is the least squares solution to the inverse problem $d = Gm$

Bibliography

[1] Bischof, J., (2000), *Ice drift, ocean circulation and climate change*, Springer-Praxis books in environmental sciences, Springer-Verlag. 215 pp.

[2] Colony, R. and Thorndike, A., (1984), *An estimate of the mean field of Arctic sea ice motion*, Journal of Geophysical Research: Oceans, Vol. 89, pp. 10623-10629

[3] Coachman, L. and Aagaard, K., (1974), *Physical oceanography of arctic and subarctic seas*, in Marine Geology and Oceanography of the Arctic Seas, edited by Herman, Y., pp. 1-72, Springer, New York

[4] Jakobsson, M. et al., (2012), *The International Bathymetric Chart of the Arctic Ocean (IBCAO) Version 3.0*, Geophysical Research Letters, Vol. 39, L12609

[5] James, G., Witten, D., Hastie, T, Tibshirani, R., (2014), *An introduction to statistical learning (with applications in R)*, Springer texts in statistics, Springer. 426 pp.

[6] Jeffries, M. et al., (2013), *The Arctic shifts to a new normal*, Physics Today, Vol. 66(10), pp. 35-40,

[7] Kimura, N. and Wakatsuchi, K., (2000), *Relationship between sea-ice motion and geostrophic wind in the Northern Hemisphere*, Geophysical Research Letters, Vol. 27, No. 22, pp. 3735-3738

[8] Kwok, R. and Rothrock, D., (1999), *Variability of Fram Strait ice flux and North Atlantic Oscillation*, Journal of Geophysical Research, Vol. 104, No. C3, pp. 5177-5189

[9] Kwok, R. and Rothrock, D., (2009), *Decline in Arctic sea ice thickness from submarine and ICESat records: 1958–2008*, Geophysical Research Letters, Vol. 36, L15501

[10] Kwok, R and Untersteiner, N, (2011) *The thinning of Arctic sea ice*, Physics Today, Vol. 64(4), pp. 36-41,

[11] Kwok, R. et al., (2013), *Arctic sea ice circulation and drift speed: Decadal trends and ocean currents*, Journal of Geophysical Research: Oceans, Vol. 118, pp. 2408-2425

[12] Lepparanta, M., (2011), *The drift of sea ice*, (2nd. ed.), Springer-Praxis Books in Geophysical Sciences, Springer-Verlag, 347 pp.

[13] Lavergne, T. et al., (2010), *Sea ice motion from space: an alternative method and its validation in the Arctic*, Proceedings to the ESA Living Planet Symposium, Bergen (Norway), 28 June - 2 July

[14] Linow, S. et al., (2013), *An analysis of the reliability of sea ice drift products calculated from SAR data*, 'ESA Living Planet Symposium 2013', Edinburgh, UK, 9–13 September 2013 (ESA SP-722, December 2013)

[15] Marshall, S., (2012), *The Cryosphere*, Princeton Primers in Climate, Princeton University press, 288 pp.

[16] Menke, W., (2012), *Geophysical Data Analysis: Discrete Inverse Theory (MatLab ed.)*, (3rd. ed.), Elsevier-Academic Press, 263 pp.

[17] Menke, W., Menke, J., (2012), *Environmental data analysis with MatLab*, Elsevier, 293 pp.

[18] Razali, N. and Wah, Y., (2011), *Power comparisons of Shapiro-Wilk, Kolmogorov-Smirnov, Lilliefors and Anderson-Darling tests*, Journal of Statistical Modeling and Analitics, Vol. 2, No. 1, pp. 21-23

[19] Rossby, C.-G. and Montgomery, R., (1935) *The layer of frictional influence in wind and ocean currents*, Papers in Physical Oceanography and Meteorology, Vol. III, No. 3 (MIT, WHOI)

[20] Rothrock, D. et al., (2008), *The decline in arctic sea-ice thickness: Separating the spatial, annual, and interannual variability in a quarter century of submarine data*, Journal of Geophysical Research, Vol. 113, C05003

[21] Sandven, S. et al., (2013), *Sea ice observing systems for Arctic science climate monitoring*, Available at http://www.arcticobservingsummit.org/aos-2013-white-papers (Accessed: 06.01.17)

[22] Spreen, G. et al, (2011), *Trends in Arctic sea ice drift and role of wind forcing: 1992–2009*, Geophysical Research Letters, Vol. 38, L19501,

[23] Thorndike, A. and Colony, R., (1982), *Sea ice motion in response to geostrophic winds*, Journal of Geophysical Research, Vol. 87, No. C8, pp. 5845-5852

[24] Wadhams, P., (2000), *Ice in the ocean*, Gordon and Breach Science Publishers. 351 pp.

[25] Weeks, W.F., (2010), *On sea ice*, University of Alaska Press. 664 pp.

[26] Wunsch, C., (1996), *The ocean circulation inverse problem*, Cambridge University Press. 442 pp.